Journal of Physiology (1995), **487.1**, *pp.*67–90

Characterization of single voltage-gated Na^+ and Ca^{2+} channels in apical dendrites of rat CA1 pyramidal neurons

Jeffrey C. Magee and Daniel Johnston

Division of Neuroscience, Baylor College of Medicine, Houston, TX 77030, USA

1. We have used dendrite-attached patch-clamp techniques to record single Na^+ and Ca^{2+} channel activity from the apical dendrites (up to 350 μm away from soma) of CA1 pyramidal neurons in rat hippocampal slices (ages: 2–8 weeks).

2. Na^+ channels were found in every patch examined (range: 2 to >20 channels per patch). Channel openings, which had a slope conductance of 15 ± 0·3 pS (mean ± S.E.M.), began with test commands to around −50 mV and consisted of both early transient channel activity and also later occurring prolonged openings of 5–15 ms. All Na^+ channel activity was suppressed by inclusion of TTX (1 μM) in the recording pipette.

3. Ca^{2+} channel activity was recorded in about 80% of the patches examined (range: 1 to >10 channels per patch). Several types of channel behaviour were observed in these patches. Single channel recordings in 110 mM $BaCl_2$, revealed an approximately 10 pS channel of small unitary current amplitude (−0·5 pA at −20 mV). These channels began activating at relatively hyperpolarized potentials (−50 mV) and ensemble averages of this low voltage-activated (LVA) channel activity showed rapid inactivation.

4. A somewhat heterogeneous population of high voltage-activated, moderate conductance (HVA_m; approximately 17 pS), Ca^{2+} channel activity was also encountered. These channels exhibited a relatively large unitary amplitude (−0·8 pA at 0 mV) and ensemble averages demonstrated moderate inactivation. The HVA_m population of channels could be tentatively subdivided into two separate groups based upon mean channel open times.

5. Less frequently, HVA, large conductance (27 pS) Ca^{2+} channel activity (HVA_l) was also observed. This large unitary amplitude (−1·5 pA at 0 mV) channel activity began with steps to approximately 0 mV and ensemble averages did not show any time-dependent inactivation. The dihydropyridine Ca^{2+} channel agonist Bay K 8644 (0·5 or 1 μM) was found to characteristically prolong these channel openings.

6. ω-Conotoxin MVIIC (10 μM), did not significantly reduce the amount of channel activity recorded from the LVA, HVA_m or HVA_l channel types in dendritic patches. In patches from somata, ω-conotoxin MVIIC was effective in eliminating a significant amount of HVA_m Ca^{2+} channel activity. Inclusion of 50 or 100 μM $NiCl_2$ to the recording solution significantly reduced the amount of channel activity recorded from LVA and HVA_m channel types in dendritic patches. A subpopulation of HVA_m channels was, however, found to be Ni^{2+} insensitive. Dendritic HVA_l channel activity was unaffected by these low concentrations of Ni^{2+}. Amiloride (1 mM) substantially reduced channel activity recorded from LVA and HVA_m channels located in dendritic patches.

7. A fairly constant density of about nine Na^+ and five Ca^{2+} channels was found in dendritic patches from adult animals. The basic profile for dendritic Ca^{2+} channel distribution was as follows: HVA_l channels were relatively restricted to the proximal 50 μm, while LVA and HVA_m channels were found with similar frequency along the length of dendrite studied.

8. A single type of TTX-sensitive Na^+ channel and at least three distinct types of Ca^{2+} channel were found at substantial densities in the apical dendrites of CA1 pyramidal neurons. The three main types of dendritic Ca^{2+} channel presented characteristics most similar to T-, R- and L-type Ca^{2+} channels. A fourth type of Ca^{2+} channel, with characteristics similar to the N-type, was also found at a lower density.

Most central neurons possess extensive dendritic arborizations that act to integrate incoming activity from thousands of excitatory and inhibitory synapses. Historically, dendrites have been considered to be passive membrane structures and quantitative descriptions of the voltage-attenuating properties of such passive structures have provided a basis for the development of theories concerning synaptic integration (for recent reviews see (Rall, Burke, Holmes, Jack, Redman & Segev, 1992; Spruston, Jaffe & Johnston, 1994). Such theories have centred around the idea that the propagation of synaptic activity through dendrites is governed solely by the anatomic and electrotonic structure of the dendritic arborization.

While the propagation of excitatory postsynaptic potentials (EPSPs) and action potentials through passive dendrites has been well described, evidence continues to accumulate suggesting that neuronal dendrites possess active properties that may participate in the integration of synaptic input. Labelling and binding studies have demonstrated the presence of Na^+ and Ca^{2+} channel antibody- and toxin-binding sites within the dendrites of several types of neurons (Westenbroek, Ahlijanian & Catterall, 1990; Westenbroek, Hell, Warner, Dubel, Snutch & Catterall, 1992; Llinás, Sugimori, Hillman & Cherksey, 1992; Mills, Niesen, So, Carlen, Spigelman & Jones, 1994). Imaging techniques have revealed substantial increases in intracellular Ca^{2+} and Na^+, presumably occurring through voltage-gated channels, following both synaptic activation and membrane depolarization (Jaffe, Johnston, Lasser-Ross, Lisman, Miyakawa & Ross, 1992; Regehr & Tank, 1992; Miyakawa *et al.* 1992). Furthermore, electrophysiological recordings of TTX-sensitive action potentials and field potentials demonstrate that Na^+ channels and perhaps other inwardly conducting voltage-gated channels are present in the dendritic regions of many central neurons (Wong, Prince & Basbaum, 1979; Miyakawa & Kato, 1986; Richardson, Turner & Miller, 1987; Turner, Meyers & Barker, 1989; Herraras, 1990; Turner, Meyers, Richardson & Barker, 1991). Some of these studies suggest that synaptic activity can open inwardly conducting voltage-gated channels and, if strong enough, initiate dendritic spike discharge (Andersen, Storm & Wheal, 1987; Turner *et al.* 1989; Herraras, 1990; Turner, Meyers & Barker, 1993; Colling & Wheal, 1994). Other studies have demonstrated that the spike initiation zone is located at the somatic-axon hillock region, and that the main function of dendritic Na^+ channels is to enhance the backward propagation of action potentials generated within this region (Turner *et al.* 1991; Stuart & Sakmann, 1994; Spruston, Schiller, Stuart & Sakmann, 1995).

If activated by synaptic inputs, dendritic voltage-gated channels could affect EPSP propagation and influence the integrative properties of neurons. Such channels could also elevate Ca^{2+} entry into dendrites, both by direct Ca^{2+} influx through voltage-gated Ca^{2+} channels or by an increased relief of Mg^{2+}-blocked NMDA channels (Mayer & Westbrook, 1987; Pongrácz, Poolos, Kocsis & Shepherd, 1992; Jaffe, Ross, Lisman, Lasser-Ross, Miyakawa & Johnston, 1994; Magee & Johnston, 1995). Elevations of postsynaptic Ca^{2+} concentration have been shown to have a profound effect on many forms of synaptic plasticity, and on the various properties of active channels themselves (Malenka, Kauer, Zucker & Nicoll, 1988; Johnston, Williams, Jaffe & Gray, 1992).

The ability of various types of stimulation to activate dendritic voltage-gated channels will depend both on the morphology and electrotonic properties of individual neurons and on the exact complement and distribution of voltage-gated channels within dendritic membrane. To further characterize these channels and to estimate their respective densities, we have used dendrite-attached, patch-clamp techniques in hippocampal slices (Stuart, Dodt & Sakmann, 1993) to record single-channel activity. Such recordings reveal the presence of a single Na^+ channel type and at least three distinct types of voltage-gated Ca^{2+} channel and provide some estimates of channel distribution.

METHODS

Preparation

Hippocampal slices (300–400 μm thick) were prepared from 2- to 8-week-old Sprague–Dawley rats, following conscious decapitation, using standard procedures (Stuart *et al.* 1993). Briefly, slices were cut on a Vibratome, incubated in a submerged holding chamber for at least 30 min at 35 °C and stored at room temperature (~22 °C) for the remainder of the experiment (< 6 h). A Zeiss Axioscope, fitted with a ×40 water-immersion objective lens and differential interference contrast (DIC) optics, was used to view slices. Light in the infrared range (740 nm) was used in conjunction with a contrast-enhancing Newvicon camera (Hamamatsu, Hamamatsu City, Japan) to better resolve individual neurons and their dendritic arbors.

Solutions and drugs

For Na^+ channel recordings the pipette solution contained (mM): 110 NaCl, 10 Hepes, either 2·5 $CaCl_2$ or 0·5 $CdCl_2$, and 100 μM 3,4 diaminopyridine (DAP) (pH 7·4 with TEAOH). For Ca^{2+} channel recordings, pipettes contained either 110 mM $BaCl_2$, 10 mM Hepes, 100 μM DAP and 1 μM TTX (pH 7·4 with TEAOH), or 20 mM $BaCl_2$, 110 mM TEACl, 10 mM Hepes, 100 μM DAP, and 1 μM TTX (pH 7·4 with TEAOH). Whole-cell recording pipettes (2–4 MΩ) were filled with (mM): 140 $KMeSO_4$, 10 Hepes, 0·5 EGTA, 3·0 $MgCl_2$, 4·0 Na_2ATP, and 0·1 TrisGTP (pH 7·4 with KOH). Standard external solutions containing (mM): 124 NaCl, 2·5 KCl, 1·2 $NaPO_4$, 26 $NaHCO_3$, 2·5 $CaCl_2$, 1·0 $MgCl_2$, and 20 dextrose, bubbled with 95% O_2–5% CO_2, were used at room temperature (~22 °C). Bay K 8644 (Calbiochem) was prepared daily from 100 mM stock solutions dissolved in DMSO. Synthetic ω-conotoxin MVIIC (Bachem, Torrance, CA, USA) was prepared from 1 mM stock solutions stored as single-use aliquots at −20 °C. Amiloride was purchased from Sigma and prepared daily. TTX (Sigma), DAP (Sigma) and lidocaine, *N*-ethylbromide quaternary salt (QX-314; Alomone, Jerusalem, Israel) were stored in aliquots, as 1 mM, 10 mM, and 0·2 M stock solutions, respectively.

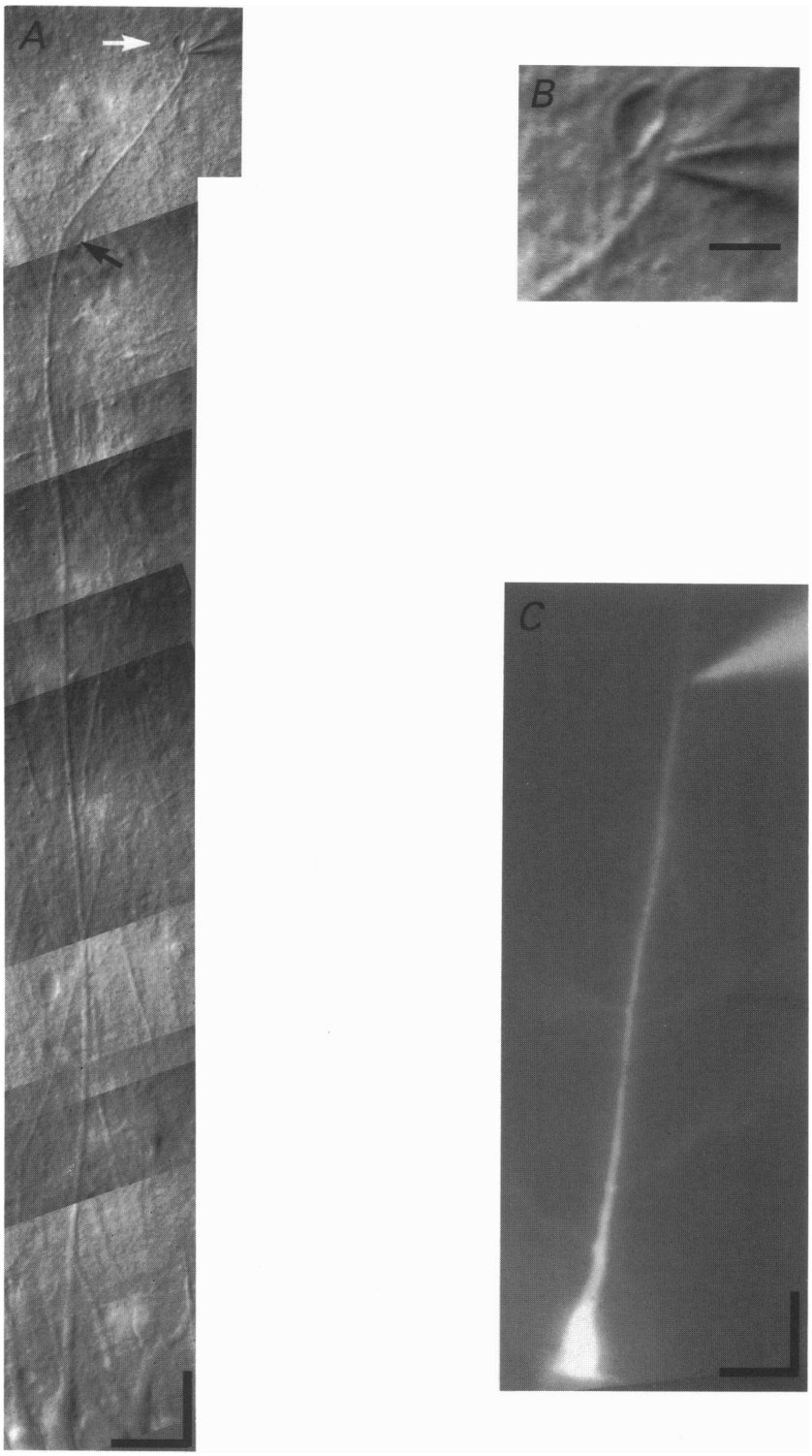

Figure 1. Cell-attached patch recordings from CA1 apical dendrites

A, differential interference contrast (DIC) image showing soma, dendrite and recording pipette 320 μm from soma (white arrow). Photos were superimposed as the dendritic regions of the neuron projected into progressively deeper focal planes. Note major dendrite branch point (black arrow). Vertical and horizontal scale bars = 25 μm. *B*, higher magnification DIC image showing recording pipette in dendrite-attached configuration. Same cell as in *A*. Scale bar = 5 μm. *C*, fluorescence image showing a CA1 pyramidal neuron that was filled with Lucifer Yellow following rupture of dendritic patch. The patch pipette containing Lucifer Yellow is 200 μm from the soma. Vertical and horizontal scale bars = 25 μm.

Recordings and analysis

Dendrites of identified pyramidal somata were visually followed 20–350 μm into stratum radiatum (Fig. 1*A*). Dendritic membrane was cleaned by a stream of solution blown from the recording electrode as it was advanced towards the cell (Stuart *et al.* 1993). Following seal formation (20–100 GΩ), Na^+ or Ca^{2+} channel activity was recorded in the cell-attached patch-clamp mode using an Axopatch 1D amplifier (Axon Instruments) (Fig. 1*B*).

Recording pipettes (6–10 MΩ), were pulled from borosilicate glass (Drummond, Broomall, PA, USA) and coated with Sylgard. Na^+ channel records were analog filtered at 2 kHz (−3 dB; 8 pole Bessel) and digitized at 20 kHz and Ca^{2+} channel records were analog filtered at 2 or 1 kHz and digitized at 10 kHz. Data were acquired using either a Masscomp 5400 or a NeXT computer using a 12-bit A/D converter (IO Tech, Cleveland, OH, USA). Data acquisition and analysis software were written in Basic-68. The resting membrane potential (V_m; −60 to −70 mV) was determined in the majority of cells by either later rupture of the patch to whole-cell recording mode or by simultaneous voltage recordings from the soma with a second whole-cell patch pipette (Axoclamp 2A amplifier). V_m measurements were taken immediately following patch rupture. The high access resistance (> 50 MΩ) of the dendritic recordings prevented rapid dialysis of the neuron by the pipette solution, such that significant changes in V_m and action potential waveforms took longer than 30 s to occur. The presence of action potentials and synaptic potentials confirm that recordings were not from presynaptic terminals or overlying glia. Also, upon rupture of the dendritic patch, several cells were filled with the fluorescent dye Lucifer Yellow (5 mg ml^{-1}), further confirming that the recordings were from CA1 pyramidal neurons (Fig. 1*C*).

Leakage and capacitive currents were digitally subtracted by averaging null traces or scaling traces of smaller amplitude. For the determination of slope conductances, current amplitude histograms were used, when possible, to determine unitary current amplitude at different voltages. Such plots were of limited use in determining slope conductance for the low voltage-activated (LVA) Ca^{2+} channels, due to difficulties in obtaining separable noise and channel opening distributions. In such cases, unitary current amplitude was calculated as the mean of single-channel amplitude determined by visual inspection of traces and hand placement of amplitude cursors. Where relevant for generation of steady-state activation and inactivation curves, fractional open times (NP_o) were calculated using $NP_o = t_o/t$ where N is the number of channels in a patch, P_o is the probability of a single channel being open during the test pulse, t_o is the time during the trace that a channel is open, and t is the total test pulse duration. NP_o for each holding potential is expressed as a fraction of maximal NP_o. For Na^+ steady-state activation curves chord conductance was calculated from the peak amplitude of ensemble currents and expressed as a fraction of the maximum. Steady-state activation and inactivation plots were fitted using single Boltzmann equations of the form:

$$y = 1/[1 + \exp((V_{½} - V)/k)]$$

and

$$y = 1 - [1 + \exp((V - V_{½})/k)],$$

where $V_{½}$ is half-maximum voltage and k is the slope factor, respectively. For channel open times, a threshold level of 50% unitary current amplitude was set for the determination of channel opening and closing transitions. When current amplitude crossed this threshold the event was counted as a transition. Durations of channel openings were accumulated in histograms and these distributions were fitted with non-linear curve fitting routines.

The minimum number of (functional) channels in a patch was estimated by dividing the maximum channel current overlap by the unitary current amplitude. For Na^+ channels we also estimated channel number by fluctuation analysis (Sigworth, 1980), and both techniques gave similar values. Care was taken throughout the course of these experiments to insure that pipette geometry, and therefore patch area, was maintained as constant as possible. Each pipette tip was carefully examined under high magnification (see Fig. 1*B*). Also, no systematic differences in the amount of suction required for seal formation were observed for dendritic or somatic recordings. All curves were fitted using non-linear least-squares programs based on the Marquardt–Levenberg algorithm. Data are expressed as means ± standard error of the mean (S.E.M.). One-way analysis of variance (ANOVA) combined with the Fisher multiple range test was used to test for drug effects on channel activity. $P < 0.05$ was considered statistically significant.

RESULTS

Dendritic Na^+ channels

Na^+ channel activity, as identified by inward-current polarity, voltage-dependent channel gating, and unitary current amplitude, was recorded from the apical dendritic regions of CA1 pyramidal neurons in a dendrite-attached patch mode. Channel activity was suppressed by inclusion of TTX (1 μM; $n = 5$) in the recording pipette or by addition of QX-314 (2 mM; $n = 2$) to the cell interior from a second pipette in the whole-cell mode on the soma. Pipette solutions containing $CdCl_2$ (0·5 mM; $n = 7$) had no effect on channel activity. Na^+ channels were found in every patch and more than a single channel was always present (range: 2 to > 20 per patch). Channel openings began with test commands to around −50 mV and consisted of both early transient channel activity and also more prolonged openings of 5–15 ms, which occurred at any time during the course of depolarization. At more hyperpolarized test potentials, channels frequently reopened several times before inactivating. The term channel 'reopenings' is used only when there are obviously more distinct channel openings than the estimated number of channels in the patch (e.g. see the fifth trace in Fig. 2*A*). With increasing depolarization the brief initial openings became more synchronized and repetitive reopenings became less frequent (Fig. 2*B*). Occasional channel openings were encountered as late as 100 ms after initial depolarization (Fig. 2*D*). As shown, these openings were mainly of the prolonged type but transient channel openings were also recorded. Slope conductance, as calculated from current-voltage (I–V) plots, was 15 ± 0·3 pS ($n = 21$), and the mean extrapolated reversal potential was +54 ± 1 mV (Fig. 3*A*). No differences were found to exist between the slope conductances of the initial transient channel activity and the more prolonged channel openings. Similar single-channel conductances and reversal potentials have been reported for Na^+ channels from a wide variety of neurons (Kirsch & Brown, 1989; Alzheimer, Schwindt & Crill, 1993). The extrapolated

reversal potential reported above is near the calculated Nernst potential assuming an intracellular Na^+ concentration of 10 mM.

Ensemble averages of greater than fifty consecutive current sweeps were used to examine the time-dependent inactivation of dendritic Na^+-channels. Ensemble averages reflected single-channel activity, such that with increasing depolarization, ensemble current amplitude became larger and inactivation more rapid. In four of seven patches, ensemble current inactivation was best fitted by the sum of two exponentials (Fig. 2*C*) suggesting two gating modes as previously shown for somatic Na^+ channels (Kirsch & Brown, 1989; Alzheimer *et al.* 1993). It seems probable that the transient, rapidly inactivating channel openings, described above, contribute to the fast time constant (τ_1) of the ensemble currents, while the more prolonged channel openings underlie the slow time constant (τ_2). Mean inactivation time constants were: $\tau_1 = 4{\cdot}6 \pm 0{\cdot}2$ ms, $\tau_2 = 48 \pm 8{\cdot}2$ ms (−40 mV); $\tau_1 = 1{\cdot}6 \pm 0{\cdot}3$ ms, $\tau_2 = 7{\cdot}1 \pm 1{\cdot}0$ ms (−30 mV); $\tau_1 = 1{\cdot}0 \pm 0{\cdot}2$ ms, $\tau_2 = 5{\cdot}8 \pm 1{\cdot}4$ ms (−20 mV); $n = 4$. These time constants are within the range of those reported for central neurons thought to possess Na^+ channels capable of alternating between two modes of gating (Kirsch & Brown, 1989; Alzheimer *et al.* 1993).

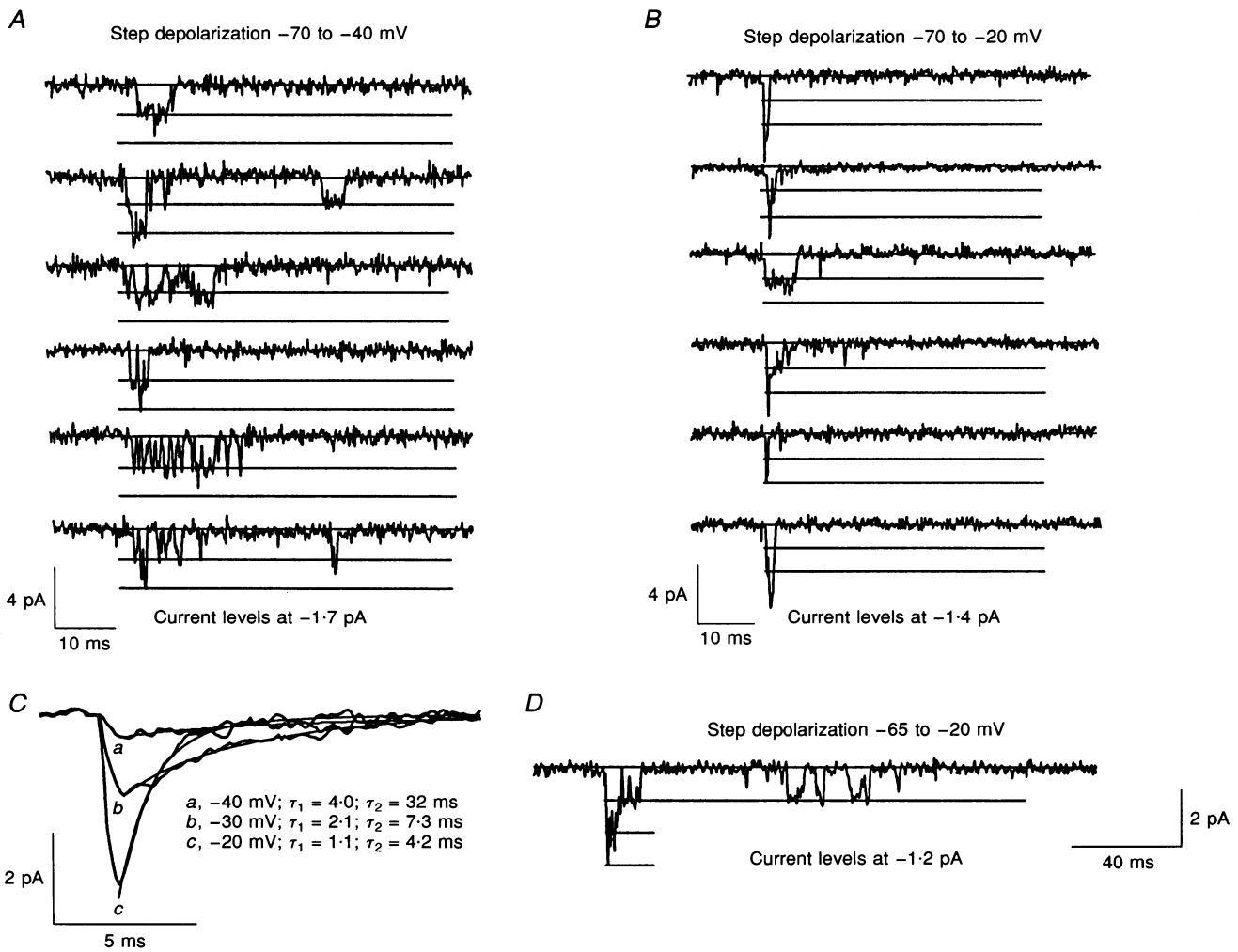

Figure 2. Dendritic Na^+ channel activity

A, consecutive sweeps of Na^+ channel activity following step depolarizations from −70 to −40 mV. Channel openings consisted of both early transient channel activity and also later occurring prolonged openings of 5–15 ms. *B*, consecutive sweeps of Na^+ channel activity following step depolarizations from −70 to −20 mV. Note that channel openings are more synchronized with the beginning of the step and inactivation is more rapid. *C*, ensemble averages of steps to: *a*, −40 mV (average of 64); *b*, −30 mV (average of 64); and *c*, −20 mV (average of 33) from −70 mV. Smooth curves represent least-squares fits of ensemble currents to a double exponential function. *D*, late-occurring Na^+ channel activity, following step depolarizations from −65 to −20 mV. Unitary current amplitude of these channels was similar to that of the early channel activity. This late channel activity was recorded at several other test voltages and the calculated slope conductance (16 pS) was also similar to that of the early channel activity (14 pS). All recordings shown were analog filtered at 2 kHz and have capacitive and leak currents subtracted.

The voltage ranges of activation and inactivation were determined for dendritic Na^+ channels through the generation of steady-state activation and inactivation curves. Steady-state activation was examined by holding patches at approximately −90 mV and subsequently stepping to various test potentials (−60 to 0 mV) in 10 mV increments. Ensemble averages were generated at each test potential (V_t) and relative chord conductance was plotted as a function of V_t (Fig. 3*B a* and *c*). Individual steady-state activation curves were well fitted by Boltzmann functions with mean $V_{½}$ and k values equal to $-30 \pm 1{\cdot}7$ mV and $6 \pm 0{\cdot}5$ ($n = 7$), respectively. Steady-state inactivation curves were generated by holding patches at various potentials ranging from −105 to −30 mV and subsequently

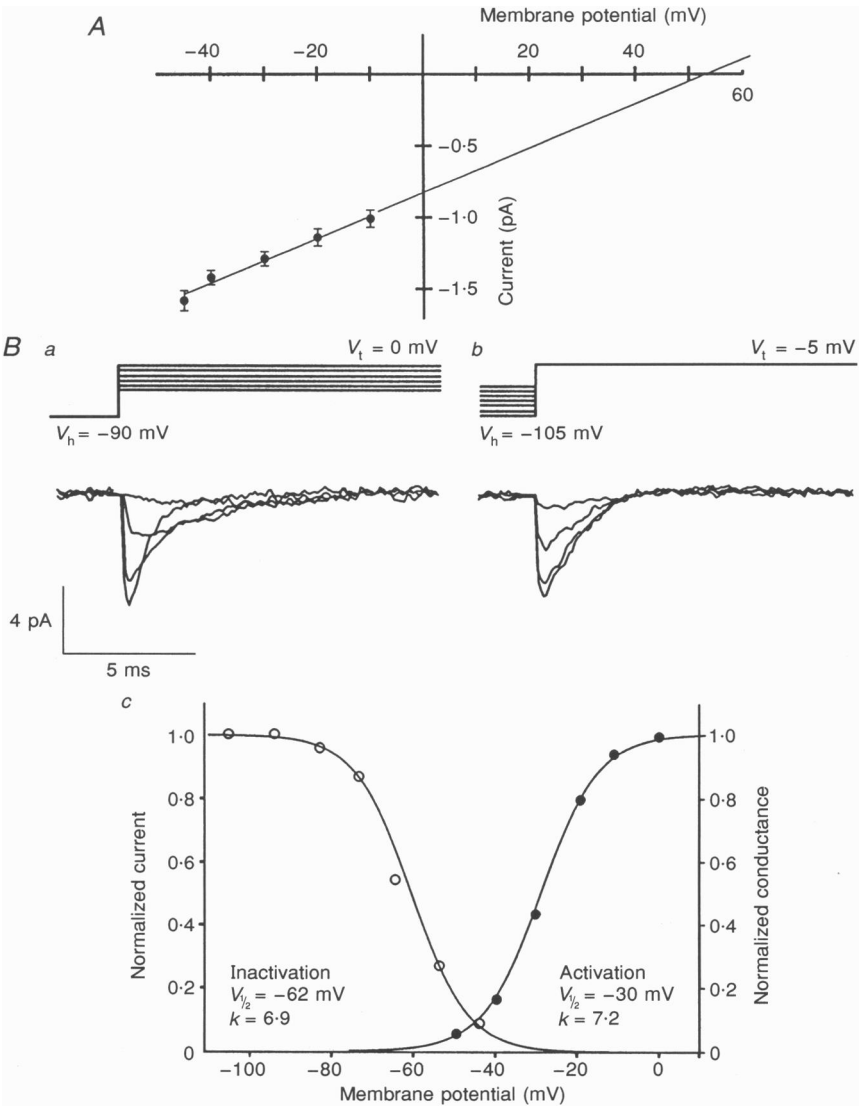

Figure 3. Dendritic Na^+ channel electrophysiology

A, *I–V* plot of Na^+ channel activity. Unitary current amplitude from a total of 27 patches is plotted as a function of membrane potential. Bars are standard error of the mean (S.E.M.). The linear regression line shown has a slope of 15 pS and crosses the *x*-axis at +54 mV. *B*, Na^+ channel steady-state activation and inactivation. *a*, ensemble averages (30–65 current sweeps) used to generate activation plots. Averages shown were evoked by steps to −55, −45, −35 and −25 mV (V_t), from a holding potential (V_h) of −90 mV. *b*, ensemble averages (35–65 current sweeps) used to generate inactivation plots. Averages shown were evoked by steps to −5 mV (V_t) from holding potentials (V_h) of −105, −85, −65 and −45 mV. Voltage protocols for *a* and *b* are shown above the traces (see Methods). *c*, representative steady-state activation (●) and inactivation (○) plots for dendritic Na^+ channels. For inactivation plot, peak ensemble current amplitude was normalized to maximum current amplitude and plotted as a function of V_h. For activation plot, chord conductance was calculated from peak ensemble amplitude, normalized to maximum and plotted as a function of V_t. Here, and in Figs 4, 5 and 6, lines are least-squares fits of the data to Boltzmann equations.

Table 1. Dendritic single-channel properties

			Activation			Inactivation					
	γ (pS)	Open time (ms)	Range (mV)	$V_{½}$ (mV)	k	Range (mV)	$V_{½}$ (mV)	k	τ (ms)	Distinctive pharmacology	Likely correlate
Na^+	15 ± 0·3	n.d.	−50 to 0	−30	6	−90 to −30	−67	7	1*‡	TTX	TTX-sen Na^+
LVA Ca^{2+}	10 ± 0·4	~1*	−55 to −5	−32	7	−100 to −40	−70	6·5	~50*	Low $[Ni^{2+}]$	T-type Ca^{2+}
HVA_m Ca^{2+}	17 ± 1	< 0·5	−20 to +30	+3	8	−80 to −15	−39	9·2	~100	Low $[Ni^{2+}]$	R-type Ca^{2+}
HVA_m Ca^{2+}	17 ± 1	~1	−10 to +30	n.d.	n.d.	−80 to −30	n.d.	n.d.	~100	Conotoxin	N-type Ca^{2+}
HVA_l Ca^{2+}	27 ± 3	< 0·5 and > 1†	−10 to +30	+9	6	n.d.	n.d.	n.d.	none	Bay K 8644	L-type Ca^{2+}

All channel properties determined at +10 mV unless otherwise specified. Ca^{2+} channel γ was determined in 110 mM $BaCl_2$ and all other properties in 20mM $BaCl_2$. γ, single-channel conductance; n.d., not determined; * determined at −20mV; † majority showed two open states; ‡ only fast τ shown; sen, sensitive.

stepping to approximately −10 mV. For inactivation plots, ensemble current amplitude or fractional open time (for those patches containing only a few channels), were plotted as a function of holding potential (V_h) (Fig. 3*Bb* and *c*). Again, individual plots were well fitted with Boltzmann functions and mean steady-state inactivation $V_{½}$ and k values were found to be −67 ± 3·2 mV and 7 ± 1·0 ($n = 5$), respectively (Table 1). The steady-state activation and inactivation parameters reported here are similar to those previously published for CA1 pyramidal neurons as well as for Na^+ currents recorded from many other types of neurons (Sah, Gibb & Gage, 1988; Ogata & Tatebayashi, 1990). These data reveal that TTX-sensitive Na^+ channels, similar in basic characteristics to many other neuronal Na^+ channels, are present in the apical dendrites of CA1 pyramidal neurons.

Dendritic Ca^{2+} channels

Ca^{2+} channel activity was also identified by inward-current polarity, voltage-dependent channel gating, unitary current amplitude, and by single-channel kinetics. Channel activity was suppressed by addition of 0·5 mM $CdCl_2$ ($n = 5$) in the pipette, while 1 μM TTX ($n = 35$) in the pipette or 2 mM QX-314 ($n = 5$) inside the cell were without effect. Ca^{2+} channels were found in about 80% of patches examined, and sometimes patches containing only a single channel were encountered (range: 1 to >10 channels per patch). Several types of channel behaviour were observed in these patches.

Dendritic Ca^{2+} channel electrophysiology

Low voltage-activated channels

In a majority of patches containing Ca^{2+} channel activity (35 of 37), we recorded from channel types that had slope conductances ranging from 7 to 20 pS in 110 mM Ba^{2+} and from 5 to 17 pS in 20 mM Ba^{2+}. Two distinct types of channel activity predominated. The first type of channel activity was considered to be from a LVA channel, as channel openings of small unitary amplitude (Fig. 4) began with command pulses to around −35 mV (110 mM Ba^{2+}). Consecutive sweeps of LVA channel activity are shown in Fig. 4*A*. As seen in these sweeps, channel openings were primarily grouped near the beginning of the depolarizations and ensemble averages of single-channel openings demonstrated significant inactivation during 60 ms step depolarizations (τ, ~50 ms at −20 mV). Individual openings of these channels were somewhat prolonged, and, as the histogram in Fig. 4*B* illustrates, channel open times were exponentially distributed. This distribution was well fitted by a single exponential function with a time constant of 1·1 ms (test potential: −15 mV). As mentioned above, channel openings were of small unitary current amplitude and *I–V* plots of LVA channel activity demonstrate that slope conductances were similarly low, ranging from 7 to 11 pS ($n = 13$; 110 mM Ba^{2+}; Fig. 4*C*).

The voltage dependence of channel activation and inactivation was investigated in a manner similar to that for Na^+ channels. In this case, steady-state activation and inactivation plots were generated by plotting NP_o, normalized to maximum, as a function of either test (activation) or holding (inactivation) potential. When 20 mM Ba^{2+} was used as charge carrier, activation of LVA channels increased rapidly over a membrane potential range of −50 to −5 mV, and steady-state inactivation varied in a graded fashion for holding potentials that ranged from −100 to −40 mV. A representative plot of these relatively hyperpolarized voltage ranges of activation and inactivation are shown in Fig. 4*D*. For this neuron, somatic voltage was simultaneously recorded by a second whole-cell pipette. The data points of the steady-state activation and inactivation plots were well fitted by Boltzmann functions and two other patches exhibited similar voltage ranges. The voltage range of activation was found to be shifted approximately 15 mV in the depolarized direction when 110 mM Ba^{2+} was used as the charge carrier, and it is assumed that the inactivation range would shift in a likewise manner. As a reference, the activation range for LVA channel activity recorded in 110 mM Ba^{2+} is shown as a dashed line in Fig. 4*D* (data from patch shown in Fig. 4*A*). These data indicate that small

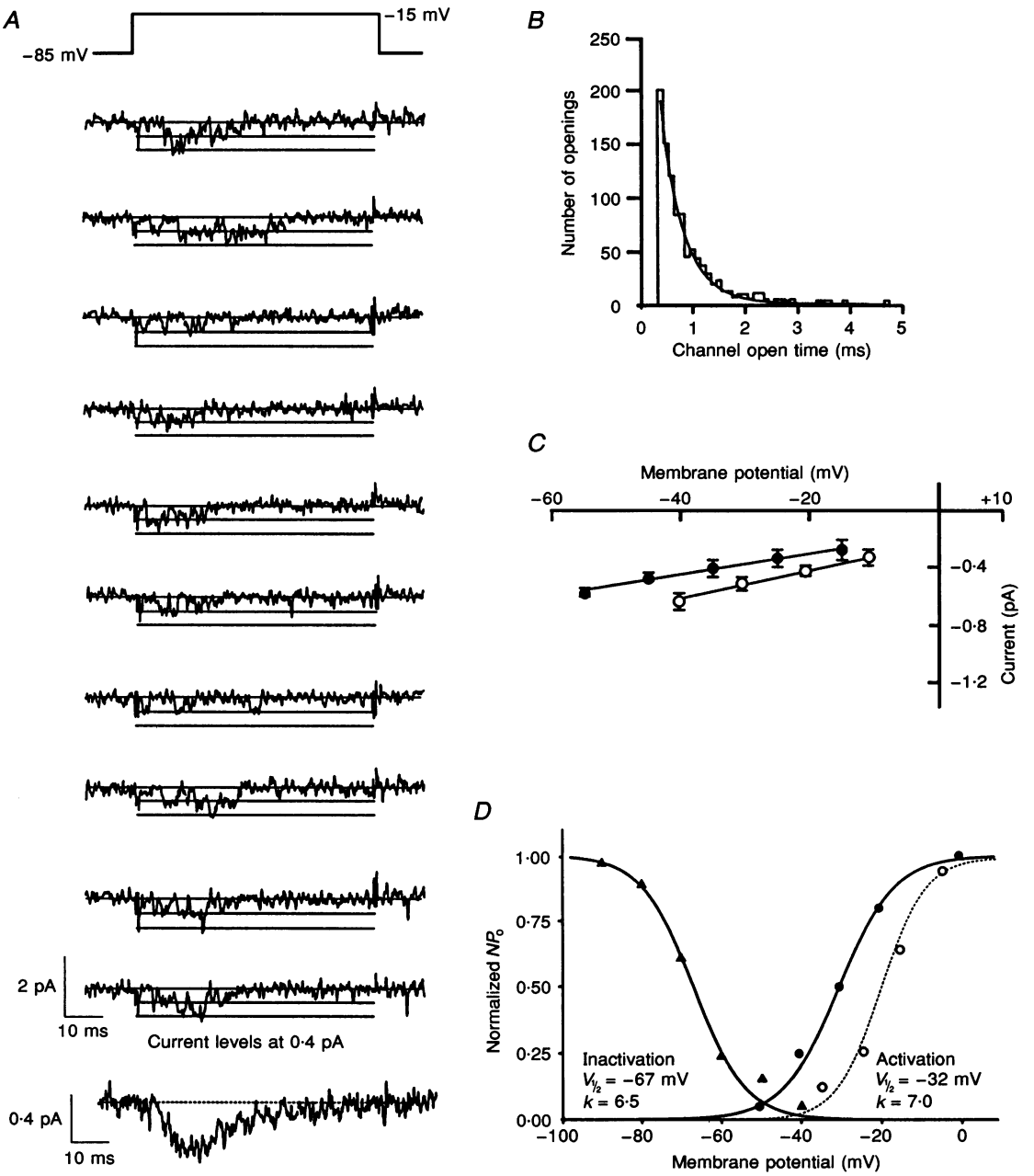

Figure 4. Dendritic low voltage-activated Ca^{2+} channel activity

A, consecutive sweeps of LVA small slope conductance (10 pS) Ca^{2+} channel activity, following step depolarizations from −85 to −15 mV. Channel openings began with command pulses to around −30 mV. Bottom trace is the ensemble average (104 traces) demonstrating significant inactivation during 60 ms depolarization. Recordings were analog filtered at 2 kHz and were later digitally refiltered at 1 kHz for display. [Ba^{2+}] in recording solution was 110 mM. *B*, channel open time histogram for same patch as in *A*. Open time distribution was best fitted by a single exponential function (τ = 1·1 ms) demonstrating that the LVA channels had a relatively prolonged mean channel open time. Raw recordings, analog filtered at 2 kHz, were used for determination of channel open times (see Methods). *C*, *I–V* plot of LVA Ca^{2+} channel activity. Unitary current amplitude is plotted as a function of membrane potential for patches recorded with either 20 mM (●, n = 27) or 110 mM (○, n = 16) Ba^{2+} as charge carrier. Bars are S.E.M. The linear regression lines shown have a slope of 8 pS (20 mM Ba^{2+}) and 10 pS (110 mM $BaCl_2$). *I–V* plots demonstrate that these channels were small conductance LVA Ca^{2+} channels. *D*, representative steady-state activation (●) and inactivation (▲) plots for dendritic LVA Ca^{2+} channels recorded in 20 mM $BaCl_2$. ○, activation range for the LVA channel activity shown in *A*. For this channel activity, which was recorded in 110 mM $BaCl_2$, $V_{½}$ and k were −19 mV and −6·5, respectively. For all plots, fractional open time (NP_o) was normalized to the maximum NP_o and plotted as a function of either V_h (inactivation) or V_t (activation).

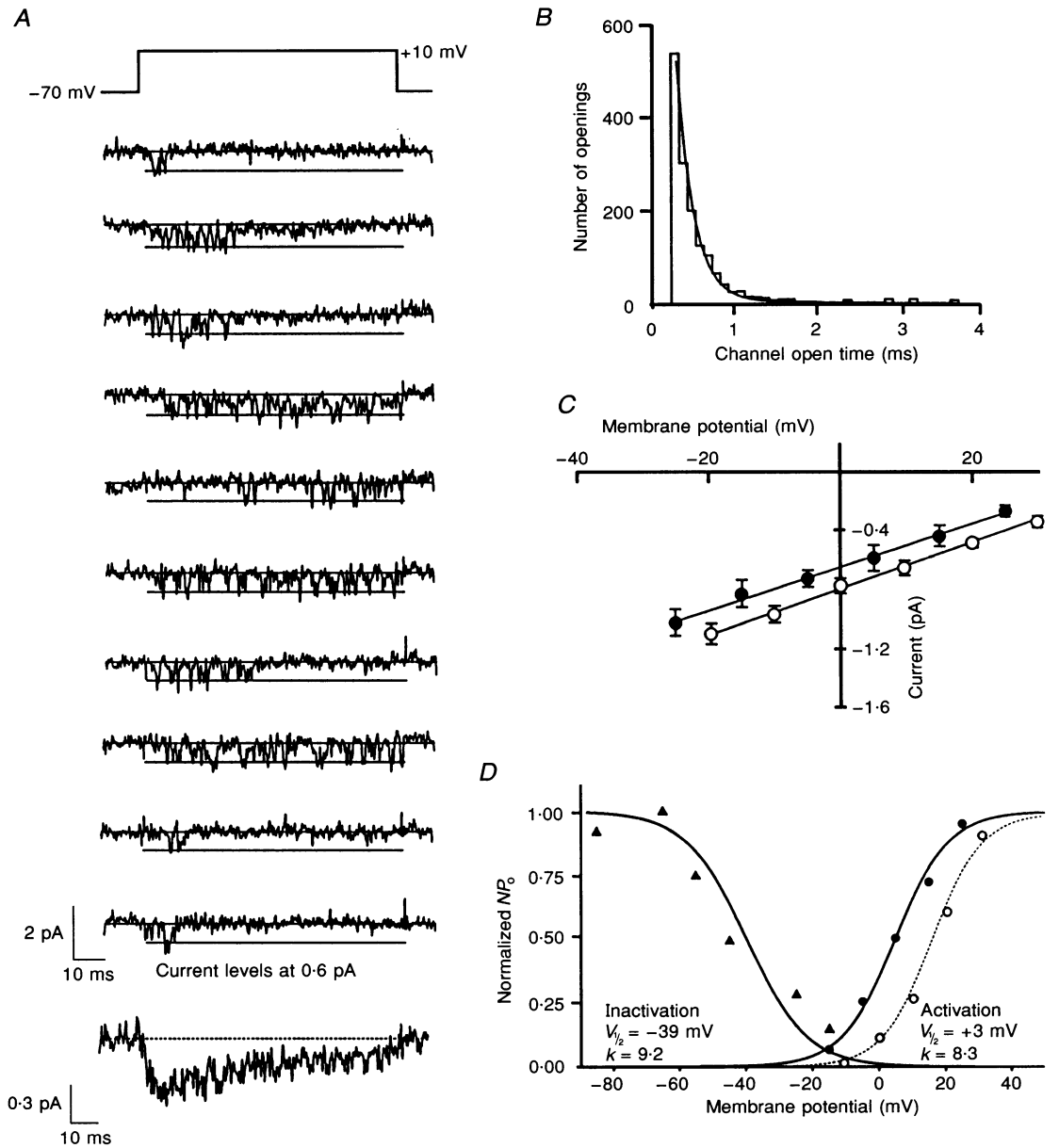

Figure 5. Dendritic high voltage-activated Ca^{2+} channel activity

A, consecutive sweeps of high voltage-activated, moderate conductance (HVA_m; 16 pS) Ca^{2+} channel activity, following step depolarizations from −70 to +10 mV. Channel openings began with command pulses to around −10 mV and were mainly transient openings with frequent reopenings. Bottom trace is the ensemble average (84 traces) showing moderate inactivation during a 70 ms depolarization. Recordings were analog filtered at 2 kHz and were later digitally refiltered at 1 kHz for display. [Ba^{2+}] in recording solution was 110 mM. *B*, channel open time histogram for same patch as in *A*. Open time distribution was best fitted by a single exponential function ($\tau = 0{\cdot}4$ ms) demonstrating that the HVA_m channels had a relatively brief mean channel open lifetime. Raw recordings, analog filtered at 2 kHz, were used for determination of channel open times (see Methods). *C*, *I–V* plot of HVA Ca^{2+} channel activity. Unitary current amplitude is plotted as a function of membrane potential for patches recorded with either 20 mM (●, $n = 22$) or 110 mM (○, $n = 13$) Ba^{2+} as charge carrier. Bars are S.E.M. The linear regression lines shown have a slope of 15 pS (20 mM Ba^{2+}) and 17 pS (110 mM Ba^{2+}). *I–V* plots demonstrate that these channels were HVA_m Ca^{2+} channels. *D*, representative steady-state activation (●) and inactivation (▲) plots for dendritic HVA_m Ca^{2+} channels recorded in 20 mM $BaCl_2$. Activation data from channels shown in *A* (110 mM Ba^{2+}) are plotted (○) and steady-state activation $V_{½}$ and k equalled +12 mV and 7·5, respectively (dashed line). For all plots, NP_o was normalized to the maximum NP_o and plotted as a function of either V_h (inactivation) or V_t (activation).

conductance, low voltage-activated, rapidly inactivating Ca^{2+} channels are present within the apical dendrites of CA1 pyramidal neurons. These channels have many basic electrophysiological characteristics in common with the previously described T-type Ca^{2+} channels (Fox, Nowycky & Tsien, 1987*b*; Fisher, Gray & Johnston, 1990; O'Dell & Alger, 1991; Mogul & Fox, 1991).

High voltage-activated (moderate conductance) channels

For the second type of frequently observed Ca^{2+} channel, command pulses to around −10 mV (110 mM Ba^{2+}) were necessary before any significant channel openings occurred. These high voltage-activated (HVA) channels had considerably larger unitary current amplitudes (Fig. 5) than was observed for the LVA channels. Representative recordings of this type of channel activity are shown in Fig. 5*A*. It can be seen from these records that most channel openings were quite transient with frequent channel reopenings occurring throughout the entire course of some depolarizations (see traces 4, 6, and 8 in Fig. 5*A*). Reflecting this single-channel activity, ensemble averages of consecutive sweeps of channel activity showed only moderate inactivation (τ_1, ~100 ms at +10 mV). The observation that individual channel openings were generally brief was supported by channel open time distributions that were well fitted by a single exponential function with a time constant of approximately 0·4 ms, at +10 mV (Fig. 5*B*). *I–V* plots of this type of HVA channel activity revealed moderate slope conductances that ranged from 15 to 20 pS ($n = 11$; Fig. 5*C*).

The voltage-dependent gating of these HVA channels was investigated through the generation of steady-state activation and inactivation plots. For two patches containing only HVA, moderate conductance (HVA_m) channel activity (20 mM Ba^{2+}), activation plots demonstrated that the probability of channel opening progressively increased across a voltage range of −20 to +30 mV (Fig. 5*D*). These channels displayed a large voltage range of inactivation as open probability decreased from holding potentials of −80 to −20 mV. A representative patch is shown in Fig. 5*D*. As shown by the dashed line in Fig. 5*D*, the voltage range of activation for HVA_m channels is shifted by less than 10 mV in the depolarizing direction when channels are recorded with a pipette solution containing 110 mM Ba^{2+} (activation curve for channel activity shown in Fig. 5*A*).

Along with the LVA channels, these moderate conductance, HVA, slower inactivating, Ca^{2+} channels were also regularly found in the apical dendrites of CA1 pyramidal neurons. Most of the basic electrophysiological characteristics of these channels are similar to those described for N-, Q-, or R-type Ca^{2+} channels (Fox *et al.* 1987*b*; Fisher *et al.* 1990; Zhang *et al.* 1993; Sather, Tanabe, Zhang, Mori, Adams & Tsien, 1993; Randall & Tsien, 1995). This channel activity is not likely to be from P-type Ca^{2+} channels, as such channels display very little time-dependent inactivation when recorded in either the whole-cell and cell-attached mode (Mintz, Adams & Bean, 1992; Usowicz, Sugimori, Cherksey & Llinás, 1992; Llinás *et al.* 1992). Also, the mostly brief channel openings demonstrated by the HVA_m channels described above are quite different from the relatively prolonged openings commonly reported for N-type Ca^{2+} channels (Fox *et al.* 1987*b*; Fisher *et al.* 1990; Delcour & Tsien, 1993). HVA_m channel activity possessing more prolonged channel open times (τ, ~1·0 ms at 0 mV) were observed in at least four patches from CA1 apical dendrites, and these openings tended to be clustered towards the beginning of step depolarizations (see Fig. 9*B*). Though not rigorously investigated, channel activation and inactivation appeared to occur over a smaller voltage range with respect to the more commonly encountered channel type. Although the infrequent observation of these channels precluded a complete investigation of their basic electrical properties, these channels appear to be most similar to N-type channels. Thus, based on the biophysical properties shown above, we tentatively place the majority of HVA_m channel activity recorded from CA1 apical dendrites into either the Q- or R-type Ca^{2+} channel category. It does appear, however, that N-type Ca^{2+} channels are also present in these dendrites, although they were encountered at a lower frequency.

High voltage-activated (large conductance) channels

One final distinct type of channel activity was consistently encountered in CA1 apical dendrites. In seven of thirty-seven patches we observed channels, possessing large unitary channel amplitudes (Fig. 6), that began opening with test pulses to around 0 mV. Figure 6*A* shows consecutive sweeps of representative channel openings following step depolarizations to +15 mV from a holding potential of −65 mV. As seen in this figure, channel openings occurred throughout the entire 70 ms depolarization and ensemble averages of this channel activity showed no time-dependent inactivation. This large amplitude channel activity consisted mainly of transient openings interspersed by more prolonged openings. The open time histograms for this channel activity, as shown in Fig. 6*B*, were best fitted by the sum of two exponentials with a fast time constant equal to 0·3 ms and a slow time constant of 1·5 ms. These dual-exponential open time distributions were observed in several other patches and suggest that more than a single open state exists for these HVA channels (Fox *et al.* 1987*b*). *I–V* plots of HVA, large unitary amplitude channel openings were generated and fitted with a linear function (Fig. 6*C*). Slope conductances, as calculated from the *I–V* plots, ranged from 25 to 30 pS (110 mM Ba^{2+}; $n = 4$). This channel activity is, therefore, from HVA, large conductance Ca^{2+} channels (HVA_l).

With a Ba^{2+} concentration of 20 mM in the pipette, the probability of opening for these HVA_l channels increased

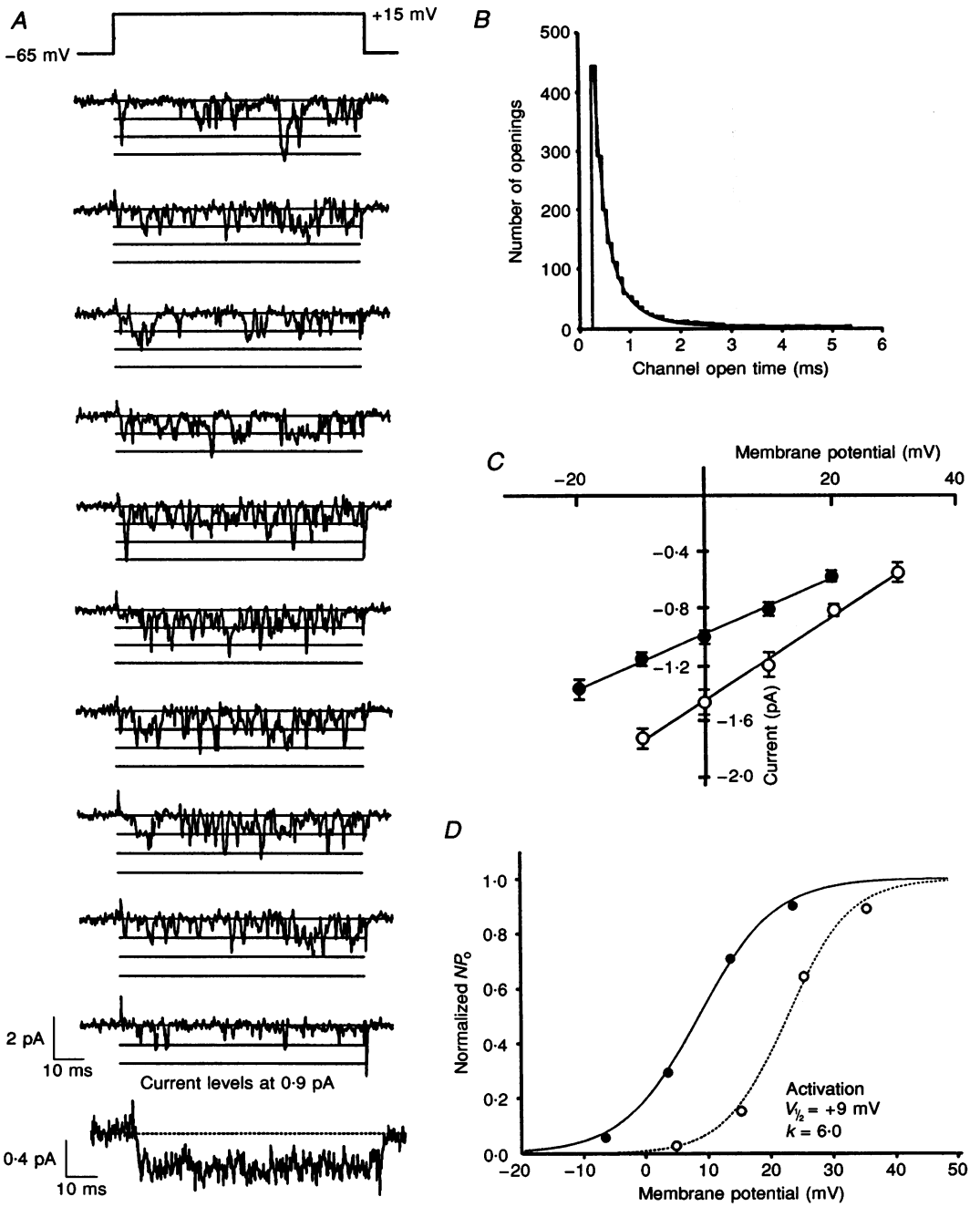

Figure 6. Dendritic high voltage-activated Ca^{2+} channel activity

A, consecutive sweeps of HVA, large conductance (HVA_1; 27 pS) Ca^{2+} channel activity, following step depolarizations from −65 to +15 mV. Channel openings began with command pulses to around 0 mV and consisted of transient openings and reopenings interspersed with relatively prolonged openings. Ensemble average (bottom trace; 60 traces) shows no inactivation during a 70 ms depolarization. Recordings were analog filtered at 2 kHz and were later digitally re-filtered at 1 kHz for display. [Ba^{2+}] in recording solution was 110 mM. *B*, channel open time histogram for same patch as in *A*. Open time distribution was best fitted by a double exponential function ($\tau_1 = 0{\cdot}3$ ms, $\tau_2 = 1{\cdot}5$ ms) demonstrating that the HVA_1 channels are capable of exhibiting either a brief mean channel open time or one that is comparatively prolonged. Raw recordings, analog filtered at 2 kHz, were used for determination of channel open times (see Methods). *C*, *I–V* plot of HVA Ca^{2+} channel activity. Unitary current amplitude is plotted as a function of membrane potential for patches recorded with either 20 mM (●, $n = 3$) or 110 mM (○, $n = 4$) Ba^{2+} as charge carrier. Bars are S.E.M. The linear regression lines shown have a slope of 23 pS (●) and 27 pS (○). *I–V* plots demonstrate that these channels were HVA_1 Ca^{2+} channels. *D*, representative steady-state activation plot for dendritic HVA_1 Ca^{2+} channels recorded in 20 mM $BaCl_2$ (●). ○, channel activity in *A* (110 mM Ba^{2+}) and for the curve shown in the dotted line, the steady-state activation $V_{½}$ and k equalled +22 mV and 6·1, respectively. For both plots, NP_o was normalized to the maximum NP_o and plotted as a function of V_t (activation).

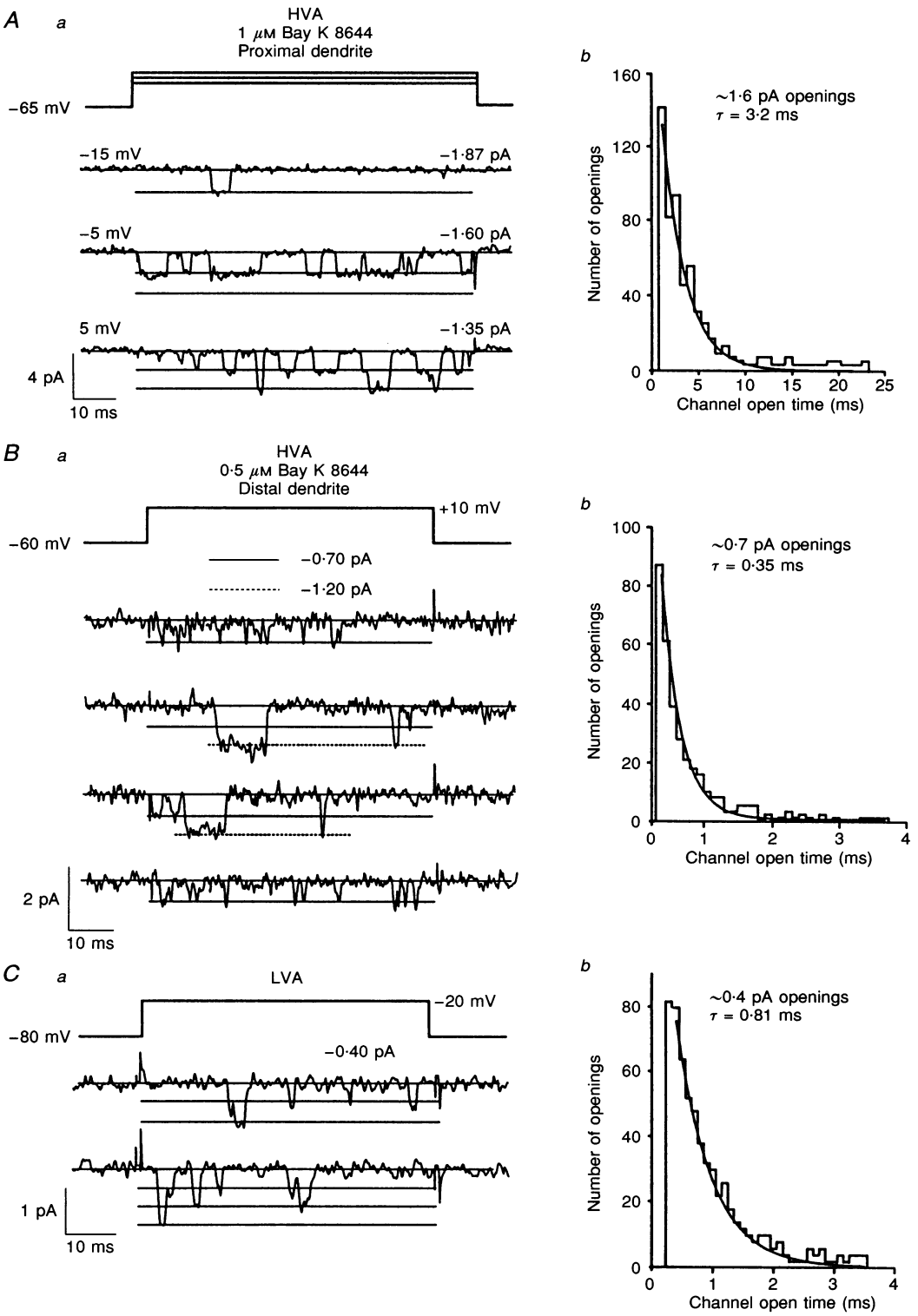

Figure 7. Effect of Bay K 8644 on dendritic Ca^{2+} channels

A, Bay K 8644 prolongs the duration of channel openings of HVA_l channels. *a*, HVA_l Ca^{2+} channel activity (slope conductance was 28 pS) following voltage steps to −15, −5 and +5 from −65 mV, with 1 μM Bay K 8644 in the pipette. Single channel openings (2–60 ms) were characteristically prolonged by Bay K 8644. *b*, channel open time distribution demonstrating that mean channel open time is increased approximately 3-fold in the presence of Bay K 8644. See Fig. 6*B* for control channel open time distribution. Smooth curve is single exponential fit of data. Patch from 40 μm out on dendrite. *B*, Bay K 8644 does not affect the channel opening kinetics of HVA_m Ca^{2+} channels. *a*, HVA channel activity, evoked by steps to +10 from −60 mV, was recorded from a dendritic patch located 160 μm from the soma with 0·5 μM Bay K 8644 in pipette. Channel activity was from both HVA_l (27 pS) and HVA_m

steeply with depolarizations ranging from −10 to +20 mV. Also, high levels of channel activity could still be recorded when the membrane patch was held at relatively depolarized patch holding potentials (−30 mV). Figure 6*D* shows a representative steady-state activation plot, using voltage protocols similar to those used above. As also shown in Fig. 6*D*, recording with 110 mM Ba^{2+} as the charge carrier resulted in a steady-state activation curve that was shifted over 10 mV in a depolarized direction (activation curve for channel activity shown in Fig. 6*A*). This HVA_l non-inactivating channel activity is very reminiscent of the L-type Ca^{2+} channels that have been well described for a variety of cell types (Nowycky, Fox & Tsien, 1985; Fox *et al.* 1987*b*; Fisher *et al.* 1990; O'Dell & Alger, 1991).

External divalent ions act to enhance the electrical field experienced by membrane-spanning ion channels by screening negative charges located on the external face of the cellular membrane. The high divalent ion concentrations used in these studies (either 20 mM or 110 mM Ba^{2+}) will theoretically shift all voltage ranges by approximately 15 and 30 mV, respectively, in a depolarized direction when compared to 2·0 mM $CaCl_2$ (Hille, 1984). The data presented, particularly from the presumed L- and T-type channels, closely approximate these theoretical calculations.

Ca^{2+} channel activity recorded in the apical dendrites of CA1 pyramidal neurons was predominately from either LVA small conductance, rapidly inactivating channels or from HVA moderate conductance, slower inactivating channels. Less frequently, HVA large conductance, non-inactivating channels were recorded in patches obtained from apical CA1 dendrites. A great diversity of Ca^{2+} channel types exist within the various neurons of the central and peripheral nervous systems. At least four distinct types of Ca^{2+} channels have been shown to be present in somata of CA1 pyramidal neurons and this diversity is preserved in the dendrites of these neurons (Hillyard *et al.* 1992). From the biophysical data presented above it appears that LVA channels, similar in basic characteristic to the 'classic' T-type channel and HVA channels similar in basic characteristics to one or more of the HVA_m channel types (most likely Q- or R-type channels) predominate in CA1 apical dendrites. Lastly, HVA_l channels reminiscent of L-type channels were occasionally encountered, primarily in the more proximal apical dendrites. A further elucidation of relative Ca^{2+} channel distribution will be undertaken below (see Channel densities).

Ca^{2+} channel pharmacology

A strictly electrophysiological examination of basic channel properties, as undertaken above, is capable of only crudely differentiating between the various types of Ca^{2+} channel presently known to exist in the CNS. Many of the various channel types share similar voltage ranges of activation and inactivation, slope conductances, and time courses of inactivation. The existence of subconductance channel states and multiple gating modes adds even further complexity. In light of this, a pharmacological investigation of dendritic Ca^{2+} channels was performed to further characterize these channels. Drug effects were tested in the cell-attached patch mode by comparing the amount of channel activity under control conditions (no drug) with that recorded with drug present be it in the pipette or external bathing solution. The amount of channel activity was quantified, without respect to the number of channels in a patch, by integrating leak subtracted current traces. When possible, multiple patches (up to 4) were taken from the dendrites and soma of a single neuron (Bay K 8644, $n = 3$; $NiCl_2$, $n = 3$; ω-conotoxin MVIIC, $n = 2$; amiloride, $n = 2$). In these cases, recordings with pipettes containing normal recording solution or recording solution containing blockers were alternated. All recordings were with 20 mM $BaCl_2$ as charge carrier, except those with Bay K 8644, which were with 110 mM $BaCl_2$. No channel activity was recorded from either dendritic ($n = 3$) or somatic patches ($n = 2$) when 500 μM $CdCl_2$ was present in the pipette.

Dihydropyridines

We examined the effect of the selective L-type Ca^{2+} channel agonist, Bay K 8644, on Ca^{2+} channel activity recorded with the 110 mM $BaCl_2$ pipette solution. Characteristically prolonged HVA single-channel openings (10–100 ms) were recorded from three of the twelve patches in which Bay K 8644 (1 or 0·5 μM) was present in the recording solution (Fig. 7*A*) (Nowycky *et al.* 1985; Fox *et al.* 1987*b*;

(16 pS) channels. HVA_l channels show mostly prolonged (10–50 ms) open times, while those of HVA_m channels were mainly brief. *b*, channel open time distribution for the HVA_m channel openings shown in *a*. Smooth curve is single exponential fit of data. Compare this plot with that under control conditions shown in Fig. 5*B*. This reduced (although still near the reported maximum) concentration had little antagonistic effect on the lower conductance channel types, while still maintaining a significant agonistic effect on the larger conductance channels. *C*, 0·5 μM Bay K 8644 appeared to have little effect on LVA channel activity. *a*, selected sweeps of LVA channel activity from same patch as in *B*, following voltage steps to −20 from −80 mV. These channels had a slope conductance of 10 pS and showed channel open times ranging from 1–4 ms. *b*, channel open time distribution for the LVA channel openings shown in *a*. Smooth curve is single exponential fit of data. Mean channel open time is similar to that seen under control conditions (see Fig. 4*B*). All recordings made with 110 mM $BaCl_2$ as charge carrier. All records shown were analog filtered at 1 kHz, and those in *Ca* were further digitally filtered at 0·7 kHz for presentation. Voltage protocols, with approximate holding potential, are schematically shown above current traces. Test potentials (upper left) and unitary current levels (upper right) are shown for each sweep in *A a*.

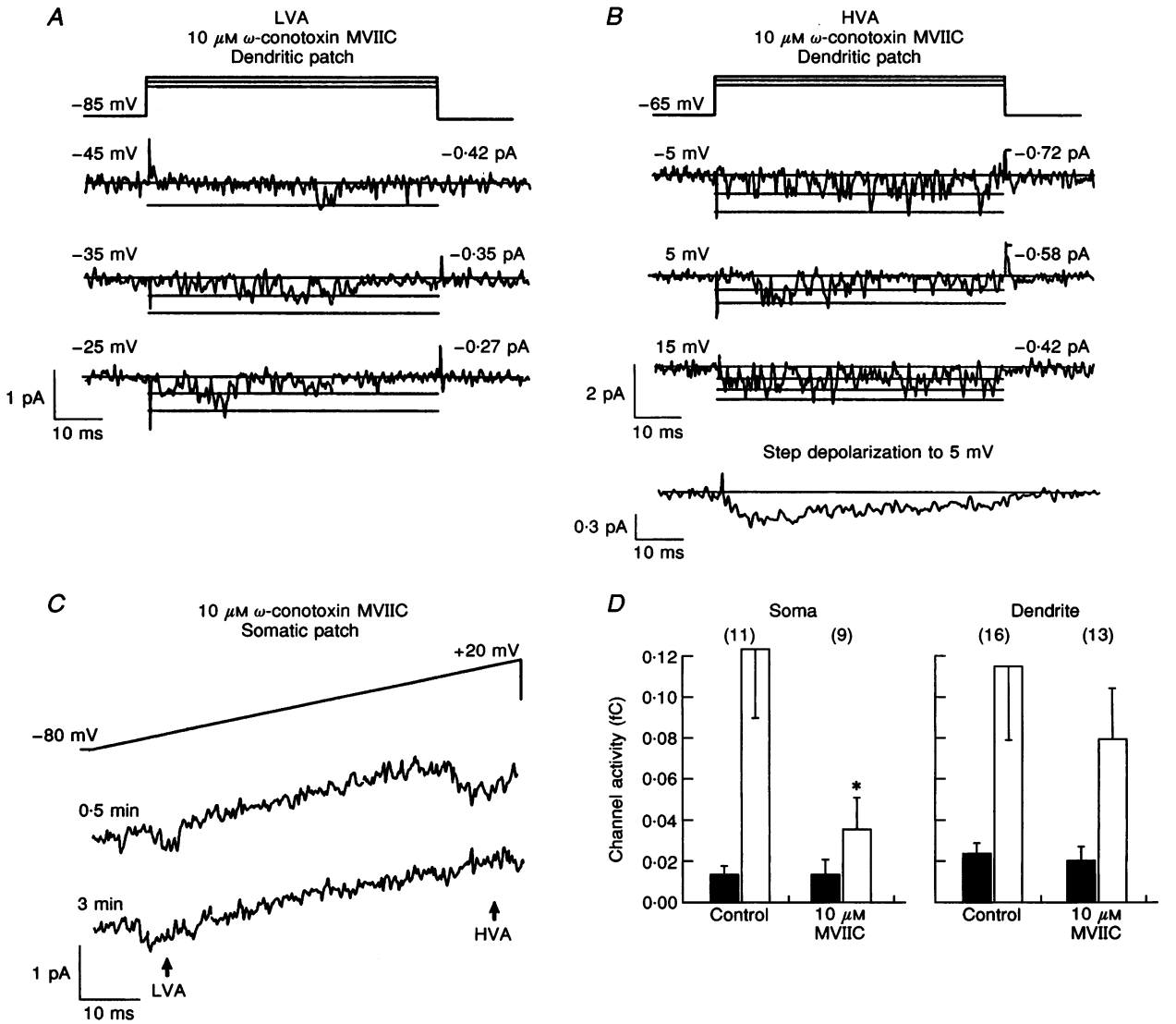

Figure 8. Effect of ω-conotoxin MVIIC on dendritic Ca^{2+} channels

A, LVA channel activity (8 pS slope conductance) following voltage steps to −35 and −25 mV from −85 mV with 10 μM ω-conotoxin MVIIC in the recording pipette. *B*, HVA channel activity (15 pS slope conductance) was also recorded with 10 μM ω-conotoxin MVIIC in pipette, following voltage steps to −5, +5 and +15 mV from −65 mV. The presence of ω-conotoxin MVIIC did not significantly reduce the amount of HVA or LVA channel activity recorded from dendritic patches. Channel openings from patches shown in *A* and *B* were recorded for 45 and 30 min, respectively, without any significant reduction in measured channel activity. *C*, ω-conotoxin MVIIC did inhibit HVA channels located on CA1 pyramidal somata. Ensemble currents (average of 5 sweeps in each) evoked by ramp depolarizations from −80 to +20 mV from a somatic patch, with 10 μM ω-conotoxin MVIIC in pipette. These records show that LVA and HVA channel openings could be recorded immediately upon gaining seal, but 3–5 min after this all HVA channel activity was absent, while LVA channel activity was still unaffected. *D*, bar plot of mean channel activity, separated into LVA (■) and HVA_m (□) types, for conditions when no channel blockers were present (Control) and for conditions when various pharmacological agents were present in the recording pipette. Channel activity is expressed as charge (fC). For this measure of channel activity, all current records following depolarizing steps to 0 mV (for HVA) and −25 mV (for LVA) were integrated and the resulting charge values averaged. The graphs show that 10 μM ω-conotoxin MVIIC significantly reduced the recorded channel activity of the HVA_m channels, when compared to control patches, only in somatic patches and did not have a significant effect on dendritic channel activity. Error bars are S.E.M. The number of patches in each group is given in parentheses above the bars. * $P < 0{\cdot}05$ for test group *versus* control group. Nifedipine (10 μM) was included in the pipette solution for all somatic recordings. All recordings were digitally filtered at 1 kHz with 20 mM $BaCl_2$ used as charge carrier. Voltage protocols, with approximate holding potential, are schematically shown above current traces. Test potentials (upper left) and unitary current levels (upper right) are shown for each sweep.

Fisher *et al.* 1990; O'Dell & Alger, 1991). The slope conductance (28 ± 4 pS) of this channel activity confirmed that these were openings of the HVA_l channel type described above. The voltage range of activation for these HVA_l channels also appeared to be shifted approximately 15 mV in a hyperpolarized direction. Such actions have also been previously reported for Bay K 8644 (Fox *et al.* 1987*b*; Mogul & Fox, 1991). No such characteristic effects were observed for patches containing only lower conductance channel types ($n = 6$; Fig. 7*B*). Unitary conductance and voltage-dependent gating properties of the LVA and HVA_m channels were unaffected by Bay K 8644, and channel open times were similar to those recorded under normal conditions (Fig. 7*Bb* and *Cb*). While lower conductance channel kinetics were unaffected by Bay K 8644, the amount of activity observed from these channel types was severely reduced. No channel activity or only very occasional low or moderate conductance channel openings were observed in several patches (for the patch shown in Fig. 7*B*, only 18 of 143 sweeps showed any channel activity). This inhibitory effect was most pronounced in 1 μM Bay K 8644, while less inhibition was observed at concentrations of 0·5 μM. For one patch containing 0·5 μM Bay K 8644, all three major channel types were easily distinguishable (Fig. 7*B* and *C*). Antagonistic actions of Bay K 8644 have been previously reported for N- and P-type channels as well as for the α_1-subunit clone, doe-I (Usowicz *et al.* 1992; Zhang *et al.* 1993). Thus, Bay K 8644 had agonistic actions only on the HVA_l channel that was found in a minority of patches. These HVA channels exhibit both electrophysiological and pharmacological characteristics of L-type Ca^{2+} channels.

ω-Conotoxin MVIIC

The recently introduced ω-conotoxin MVIIC is an effective inhibitor of N-, P-, and Q-type channels (Hillyard *et al.* 1992; Zhang *et al.* 1993; Swartz, Mintz, Boland & Bean, 1993; Randall & Tsien, 1995; although see Elmslie, Kammermeier & Jones, 1994). Also, ω-conotoxin MVIIC has been shown to block current expressed in *Xenopus* oocytes from the cloned α_{1A} and α_{1B} Ca^{2+} channel subunits (Zhang *et al.* 1993; Sather *et al.* 1993). As high concentrations of divalent cations have been reported to reduce the effectiveness of ω-conotoxin GVIA (McCleskey *et al.* 1987), we used pipette solutions containing a relatively low concentration of $BaCl_2$ (20 mM).

With 10 μM ω-conotoxin MVIIC ($n = 10$) included in the recording pipette, LVA channel activity was recorded with a frequency similar to that used when no drug was present. Ten of thirteen patches contained LVA channel activity and integration of these traces gave mean charge values of 0·024 ± 0·008 fC ($n = 13$). These values were not significantly different from control patches where LVA channels were found in thirteen of sixteen patches and mean charge values of 0·021 ± 0·005 fC were calculated (See Fig. 8*D*). LVA channel properties such as unitary conductance, activation and inactivation properties and channel kinetics were similarly unaffected by ω-conotoxin MVIIC (Fig. 8*A*). HVA_m channel activity was also recorded in seven of thirteen patches and here the mean charge equalled 0·080 ± 0·026 fC ($n = 13$). These values were not significantly different from control conditions where HVA_m channels were observed in eleven of sixteen patches (0·116 ± 0·044 fC; $n = 16$). Single-channel openings of these ω-conotoxin MVIIC insensitive channels were brief ($\tau = 0{\cdot}46$ ms; Fig. 8*B*) with frequent reopenings occasionally occurring throughout the depolarization. As seen in Fig. 8*B*, ensemble averages of channel activity displayed moderate inactivation during 60 ms step depolarizations. This channel activity was very similar to that described above, in more detail, for the more frequently encountered HVA_m channels. These results suggest that, while ω-conotoxin MVIIC did slightly reduce the observations of HVA_m channels, the channel activity occurring in these patches was not affected by ω-conotoxin MVIIC. Also, in one dendritic patch with ω-conotoxin MVIIC present in the pipette, control levels of HVA_l channel activity were recorded, suggesting that ω-conotoxin MVIIC had no effect on HVA_l channel activity recorded from CA1 dendrites. Thus, the majority of Ca^{2+} channels in CA1 apical dendrites are not ω-conotoxin sensitive N-, P- or Q-type channels.

In somatic patches, ω-conotoxin MVIIC was effective in eliminating most HVA_m channel activity ($n = 9$) over a period of time less than 3 or 4 min following seal formation. The block of single-channel openings was somewhat slower than expected, although a period of minutes is required for maximum ω-conotoxin MVIIC effect on whole-cell Ba^{2+} currents (Sather *et al.* 1993; Eliot & Johnston, 1994). As a result of this slow block all measures of channel activity were taken at 5 min following seal formation. In Fig. 8*C*, ramp depolarizations show the presence of both LVA and HVA channel activity in a somatic patch immediately following seal formation. Within 2 min of seal formation, all of the HVA channel activity was absent, while that of the LVA channels remained unchanged. Thus, as has been reported elsewhere in greater detail, CA1 somata contain a high proportion of ω-conotoxin MVIIC-sensitive channels (Hillyard *et al.* 1992; Swartz *et al.* 1993). More importantly, these results provide a positive control for the effects of 10 μM ω-conotoxin MVIIC on dendritic patches.

Nickel

Many reports have shown that most LVA or T-type Ca^{2+} channels are inhibited by relatively low concentrations (IC_{50}, ~50 μM) of $NiCl_2$ (Fox, Nowycky & Tsien, 1987*a*; Bean, 1989; Mogul & Fox, 1991; Winegar, Kelly & Lansman, 1991; Zhang *et al.* 1993). On the other hand, almost all HVA channel types (with the exception of the native R-type channel and also the α_{1E} and doe-1 Ca^{2+} channel subunit clones) are relatively unaffected by such low concentrations of Ni^{2+} (Fox *et al.* 1987*a*; Bean, 1989; Zhang *et al.* 1993; Soong, Stea, Hodson, Dubel, Vincent &

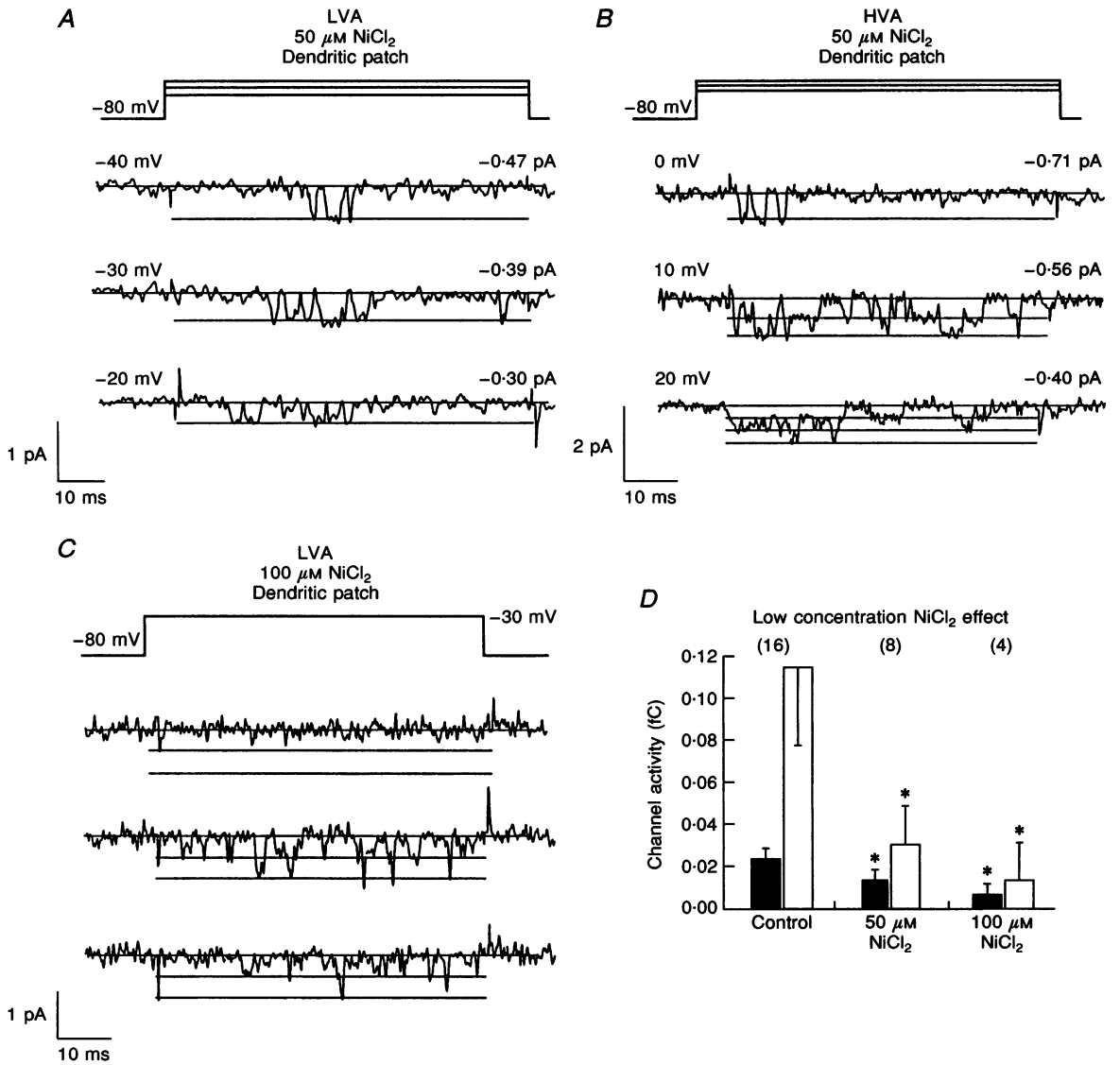

Figure 9. Effect of $NiCl_2$ on dendritic Ca^{2+} channels

A, LVA channel activity (9 pS slope conductance) following voltage steps to −40, −30 and −20 mV from −80 mV, with 50 μM $NiCl_2$ in the pipette. The presence of $NiCl_2$ reduced but did not prevent the observation of LVA channel activity. *B*, HVA channel activity (14 pS slope conductance) following voltage steps to 0, 10 and 20 mV from −80 mV, with 50 μM $NiCl_2$ in the pipette. In general, 50 and 100 μM $NiCl_2$ greatly reduced the observation of HVA channel activity in nearly all patches examined. However, 50 μM Ni^{2+}-insensitive channels were present in dendritic membrane. The HVA, moderate conductance, channel activity shown in *B* was much greater (0·14 fC) than that recorded for any other patch with $NiCl_2$ in pipette solution (the next highest was 0·02 fC). Also, the channel open times measured for this Ni^{2+}-insensitive channel activity were quite prolonged (1–10 ms) when compared to that most commonly encountered in dendritic patches (see Fig. 4*B*). *C*, LVA channel activity (9 pS slope conductance) following 3 consecutive voltage steps to −30 mV from −80 mV, with 100 μM $NiCl_2$ in the pipette. Channel openings were markedly brief and infrequent in the presence of 100 μM $NiCl_2$. *D*, bar plot of mean channel activity, separated into LVA (■) and HVA_m (□) types, for conditions when no channel blockers were present (Control) and for conditions when various pharmacological agents were present in the recording pipette. Statistical analysis demonstrates that 50 μM and 100 μM $NiCl_2$ significantly reduced the recorded channel activity of both the LVA and the HVA_m channels when compared to control patches. Error bars are S.E.M. The number of patches in each group is given in parentheses above the bars. * $P < 0·05$ for test group *versus* control group. Somatic channel activity was not significantly affected by the presence of 50 μM $NiCl_2$ ($n = 4$). All recordings were digitally filtered at 1 kHz with 20 mM $BaCl_2$ used as charge carrier. Records in *A* were also digitally filtered at 0·7 kHz for presentation. Voltage protocols, with approximate holding potential, are schematically shown above the current traces. Test potentials (upper left) and unitary current levels (upper right) are shown for each sweep in *A* and *B*.

Snutch, 1993; Ellinor *et al.* 1993*b*). We thus included low concentrations (50 and 100 μM) of $NiCl_2$ in the 20 mM $BaCl_2$ recording solution in order to test for effects on LVA channel activity.

With 50 μM $NiCl_2$ present within the recording pipette, light amounts of LVA channel activity were found in five of eight recordings (Fig. 9*A*), and integration of current traces gave mean values of $0{\cdot}014 \pm 0{\cdot}002$ fC. This represents a 46% reduction of channel activity and is significantly lower than that found in control patches ($0{\cdot}024 \pm 0{\cdot}008$ fC). LVA channel activity was reduced by 81% of control ($0{\cdot}005 \pm 0{\cdot}001$ fC; $n = 4$) when 100 μM $NiCl_2$ was included in the pipette solution (Fig. 9*D*). LVA single-channel activity, recorded in the presence of $NiCl_2$ (100 μM in particular), mainly consisted of relatively brief bursts of openings (Fig. 9*C*). Such transient openings are thought to result from channel transitions between blocked and unblocked states and are consistent with previous accounts of divalent block of Ca^{2+} channels (Hess, Lansman & Tsien, 1986; Winegar *et al.* 1991). Extremely small amounts of HVA_m channel activity were recorded from dendritic patches with 50 μM $NiCl_2$ present in the recording solution ($0{\cdot}021 \pm 0{\cdot}009$ fC; $n = 9$). Only two of eight patches showed even infrequent channel openings while a third patch exhibited normal amounts of channel activity. HVA_m channel activity from this latter patch (Fig. 9*B*) exhibited single-channel behaviour (open time $\tau = 1{\cdot}1$ ms at +10 mV) and a voltage range of activation (comparatively more depolarized) more reminiscent of N-type Ca^{2+} channels. Thus, the LVA Ca^{2+} channels recorded in the apical dendrites of CA1 neurons were sensitive to 50 μM $NiCl_2$ as were the predominant HVA_m Ca^{2+} channels. CA1 dendrites do, however, contain a lower density of Ni^{2+}-insensitive HVA_m channels that exhibit many electrophysiological characteristics of N-type channels.

The recording conditions used here may slightly reduce the ability of Ni^{2+} to block channels. As Ni^{2+} is a competitive channel blocker, which blocks by binding to the Ca^{2+} binding site within the pore, higher concentrations of permeant divalent ions (in this case, 20 mM Ba^{2+}) could theoretically overcome the channel block for a given concentration of Ni^{2+} (Hess *et al.* 1986). Thus, the high Ba^{2+} concentrations used in these studies may inhibit the channel-blocking effect of 50 μM $NiCl_2$. Ni^{2+} (50 μM) did not shorten the relatively long-duration openings (τ_1, ~1·0 ms at 0 mV) demonstrated by HVA_m channels located in somatic patches ($n = 3$).

Amiloride

Amiloride has been shown to be a somewhat selective LVA Ca^{2+} current blocker. In a variety of preparations, 200–300 μM amiloride has been shown to inhibit 50% of LVA current, while 1 mM concentrations have been used for a complete block (Tang, Presser & Morad, 1988; Mogul & Fox, 1991; Thompson & Wong, 1991). The α_{1E} Ca^{2+} channel subunit has also been reported to be inhibited by 1 mM amiloride (Schneider *et al.* 1994). The inhibitory effect of amiloride has been reported to be slow and almost completely reversible (Tang *et al.* 1988; Mogul & Fox, 1991; Thompson & Wong, 1991). The slow time course of amiloride block and unblock provide an added advantage that was exploited in the present study.

In an initial set of experiments, Ca^{2+} channel activity was recorded from the dendritic regions of CA1 neurons with 0·5 or 1 mM amiloride included in the recording solution ($n = 9$). Amiloride (0·5 mM) had a slight effect on LVA and HVA channel activity, reducing the measured openings to about half of control conditions (Fig. 10*D*). With 1 mM amiloride included in the recording pipette, very low levels of LVA and HVA channel activity (0·006 and 0·010 fC, respectively; $n = 6$) were recorded from dendritic patches 5 min after seal formation (Fig. 10*D*). Although difficult to determine with such low levels of channel activity, the HVA activity appeared to be of moderate conductance. Thus, inclusion of 1 mM amiloride into the pipette solution had a significant antagonistic effect on both LVA and HVA_m channels located in the dendrites of CA1 pyramidal neurons. No such antagonistic effect of 1 mM amiloride was observed in somatic patches, where HVA_m channel activity was similar to that recorded under control conditons ($n = 3$).

In a second set of experiments, the slow washout of amiloride block was used to provide a further test of the effects of amiloride. With 1 mM amiloride in the external bathing solution, very little channel activity could be recorded immediately following seal formation (1 min in Fig. 10*A*). However, channel activity progressively increased over time, such that at 5 min after seal formation mean channel activity had increased dramatically (5 min in Fig. 10*A*). A temporal increase in both LVA and HVA_m channel activity was observed. In another patch containing a large number of HVA_m channels (and only 1 or 2 LVA channels) ensemble averages reveal that a moderately inactivating current was initially blocked by 1 mM amiloride. Ensemble average current amplitude increased progressively for the initial 10 min of amiloride washout. Amiloride (1 mM), therefore, reversibly blocked both LVA and HVA_m channels in dendritic patches of CA1 pyramidal neurons (Fig. 10*B*).

Non-specific channel effects have been previously reported for relatively high concentrations of amiloride (0·5 mM) (Mogul & Fox, 1991). In fact, no HVA_l channel activity was recorded from either somatic or dendritic patches ($n = 9$) when amiloride was present in the recording solution. Thus the rather high concentrations of amiloride used in these studies may have had some antagonistic effects on L-type Ca^{2+} channels (see also Mogul & Fox, 1991). Amiloride has also been shown to block the Na^+–H^+ exchanger, thereby possibly affecting intracellular pH and having an indirect Ca^{2+} channel-blocking effect (Mogul & Fox, 1991). It seems

highly unlikely, however, that application of amiloride to only a tiny patch of membrane could have any significant effect on intracellular pH. Furthermore, when amiloride was included in the bathing solution, channel activity was recorded when amiloride was 'washed out' from only the membrane patch under study. Again, it would not be expected that intracellular pH would be significantly altered by such a manipulation.

To summarize, in a large majority of dendritic patches we encountered LVA, small conductance Ca^{2+} channels that were sensitive to a low concentration of Ni^{2+} and 1 mM amiloride, but were insensitive to ω-conotoxin MVIIC. In terms of both biophysical and pharmacological characteristics, the LVA channels appear to be a single population. Such uniformity was not the case for HVA_m channel activity. The predominant HVA_m Ca^{2+} channels in CA1 dendrites were low concentration Ni^{2+} and 1 mM amiloride sensitive and ω-conotoxin MVIIC insensitive. There was, however, a less frequently encountered subpopulation of Ni^{2+}-insensitive and possibly ω-

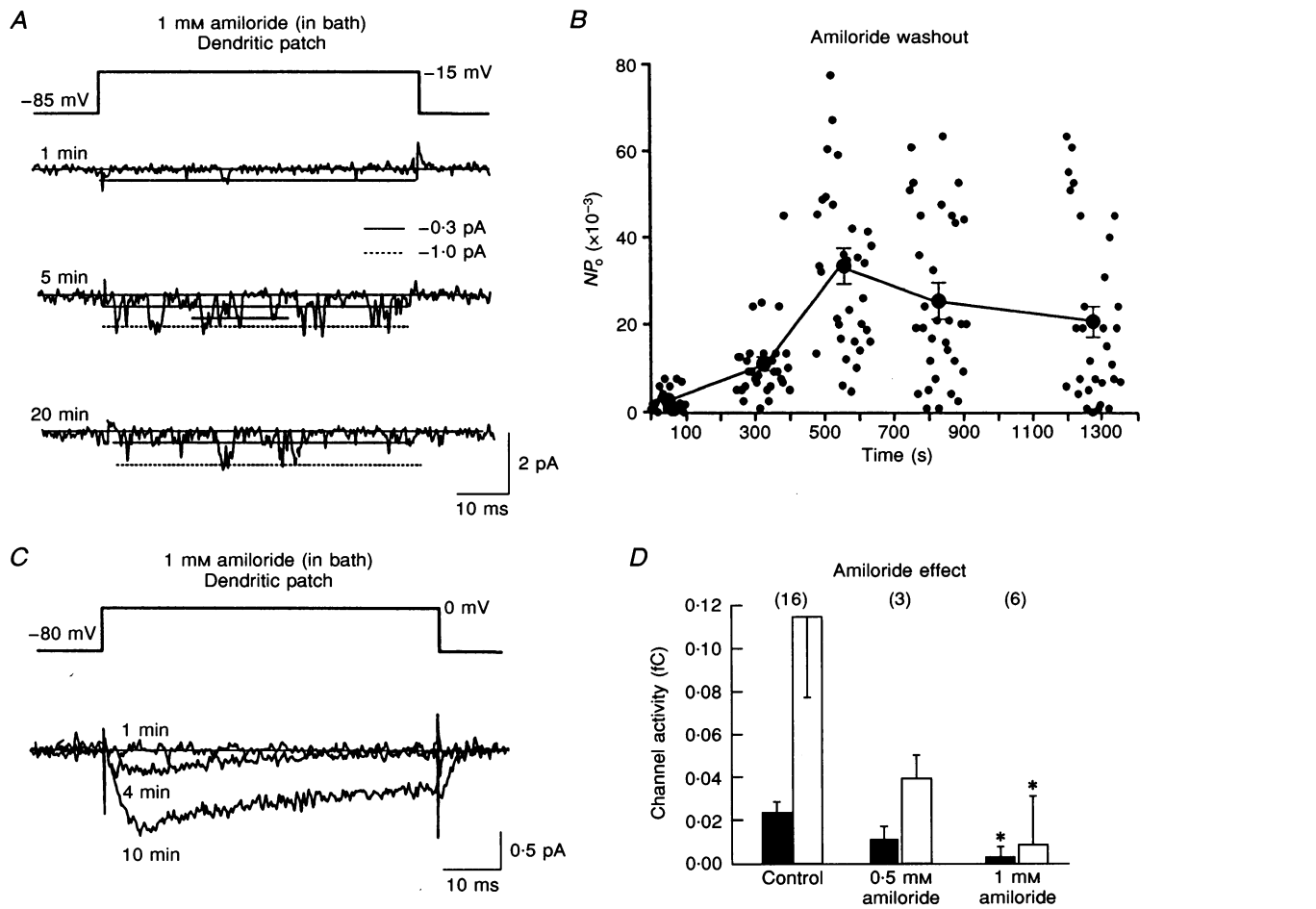

Figure 10. Effect of amiloride on dendritic Ca^{2+} channels

A, with 1 mM amiloride present in the external bathing solution, but not in the recording solution, voltage steps from −85 to −15 mV initially (1 min after seal formation) showed little channel activity. However, 5 min after seal formation, as amiloride block was washed out by pipette solution, a dramatic increase in channel activity (including both HVA_m and LVA channel types) could be recorded in response to the same voltage steps. *B*, plot of NP_o with time for patch shown in *A* demonstrating the increase of channel activity as amiloride was washed out. *C*, in another patch, ensemble average amplitude increases with time from seal formation. Voltage steps were from −80 to 0 mV (1 min is average of 25, 4 min is average of 42, and 10 min is average of 41 sweeps). *D*, bar plot of mean channel activity, separated into LVA (■) and HVA_m (□) types, for conditions when no channel blockers were present (Control) and for conditions when amiloride was present in the recording pipette. Channel activity is expressed as charge (fC). Amiloride (1 mM) significantly reduced the recorded channel activity of both the LVA and the HVA_m channels when compared to control dendritic patches. Error bars are S.E.M. The number of patches in each group is given in parentheses above the bars. * $P < 0{\cdot}02$ for test group *versus* control group. Voltage protocols, with approximate holding potential, are schematically shown above the current traces. All recordings were digitally filtered at 1 kHz with 20 mM $BaCl_2$ used as charge carrier.

conotoxin MVIIC-sensitive HVA_m channels. Finally, HVA_l dihydropyridine-sensitive Ca^{2+} channels were found in a minority of patches.

Channel densities

Na^+ channels were found in all patches throughout the entire range of dendrites studied and the distribution is shown in Fig. 11*A*. In juvenile rats (under 4 weeks of age) dendritic recordings were restricted to the first 100 μm. In these young rats, an average of $6 \pm 0{\cdot}6$ channels patch^{-1} ($n = 17$) was found, and this yields an approximate channel density of 28 ± 3 pS μm^{-2} (assuming an average patch area of 3 μm^{-2}; Stuart & Sakmann, 1994). This can be compared with an average of $9 \pm 1{\cdot}7$ channels patch^{-1} ($n = 5$) for somatic recordings yielding an approximate somatic channel density of 45 ± 8 pS μm^{-2}. Thus, in juvenile rats there appear to be fewer Na^+ channels in the dendrites than on the soma. In rats 5 weeks of age and older, the average channel density of dendritic membrane (recordings up to 350 μm) was 61 ± 7 pS μm^{-2} compared to 56 ± 15 pS μm^{-2} of somatic membrane. Therefore, Na^+ channel density increases with animal age, particularly in the dendritic regions, and the differences in channel density between these regions is reduced in adult animals. In both age groups we found little evidence of non-uniform channel distributions along the entire range of dendrites studied.

Figure 11*A*, however, shows that the greatest range of Na^+ channel density is found in the more proximal dendritic regions (< 200 μm from the soma), with three patches having a channel density more than twice the mean. These patches could represent the presence of 'hotspots' in the dendrites or simply reflect a slightly higher overall channel density in the proximal *versus* distal (> 200 μm from the soma) dendritic regions.

Ca^{2+} channels were also found in all regions of dendrites studied. The basic profile for dendritic Ca^{2+} channel distribution was as follows: HVA_l channels were relatively restricted to the proximal 50 μm, while the other two main channel types were found with similar frequency along the length of dendrite studied (Fig. 11*B*). As was found for Na^+ channels, Ca^{2+} channel density was lower in the juvenile rats compared to adults. Ca^{2+} channels were found in about 50% of patches from animals < 4 weeks of age. Across the length of dendrite studied in juvenile rats (up to 100 μm), HVA_m channel density averaged 10 ± 2 pS μm^{-2} ($n = 8$), and LVA channel density averaged 7 ± 2 pS μm^{-2} ($n = 10$) in those patches exhibiting channel activity. HVA_l channels contributed an additional average density of 10 ± 2 pS μm^{-2} ($n = 4$), to the first 50 μm of apical dendrite, while contributing very little beyond these proximal regions. In dendrites of adult rats, channels were found in about 80% of patches. For the entire extent of

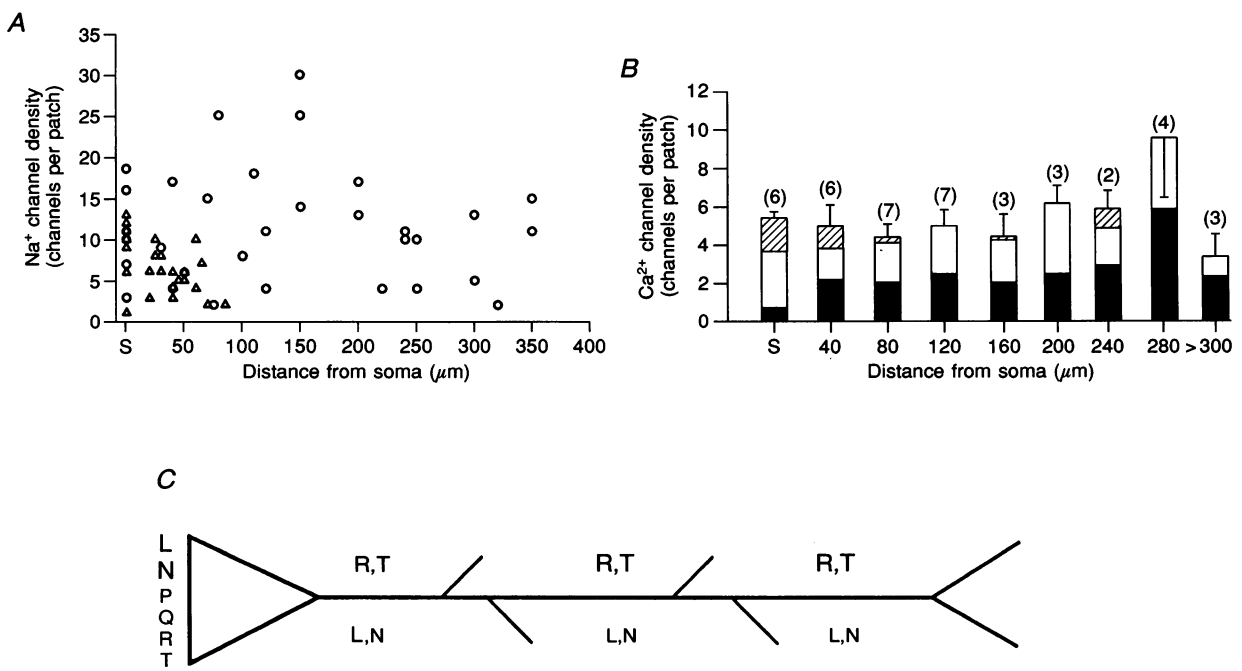

Figure 11. Dendritic channel distributions

A, Na^+ channel density plotted as a function of distance of patch from soma (S). ○, patches recorded from slices taken from rats less than 4 weeks of age, and △, recordings from slices of rats 4 weeks of age and older. *B*, bar plot of Ca^{2+} channel density as a function of distance from soma, demonstrating that channel density is fairly uniform across the length of dendrite studied. Error bars are S.E.M. for total number of channels per patch and number of patches for each are shown above the bars in parentheses. ▨, HVA_l; □, HVA_m; ■, LVA. *C*, schematic diagram of proposed Ca^{2+} channel distribution. Relative densities of different channel types are represented by font size.

CA1 apical dendrite studied in adult rats (up to 340 μm), HVA_m channel density averaged 15 ± 2 pS μm^{-2} ($n = 26$), and LVA channel density averaged 10 ± 2 pS μm^{-2} ($n = 29$) in those patches exhibiting channel activity. HVA_l channels contributed an additional average density of 12 ± 2 pS μm^{-2} ($n = 4$) to the first 50 μm of apical dendrite. Thus, the same types of voltage-activated Na^+ and Ca^{2+} channels are found in juvenile and adult CA1 apical dendrites, yet the density of channels in dendritic membrane of adults is about double that of juveniles. In four recordings from adult neurons (2 from the main trunk and 2 from branch points), and one recording from a 17-day-old rat, more than 15 Ca^{2+} channels were observed in patches from apical dendritic regions (recording sites ranged from 70 to 250 μm). This density of channels is severalfold over that of the mean and could represent some type of channel clustering. In all cases other than these five recordings, dendritic Ca^{2+} channel density was less than that of Na^+ channel density.

All of the recordings from CA1 dendrites reported here are from the main trunk or at best one or two branches off the trunk (dendrite diameter $>1{\cdot}5$ μm). In light of this, the channel densities of smaller dendritic regions, such as radial oblique branches, could be substantially different to those reported here.

DISCUSSION

Dendritic Na^+ channels

TTX-sensitive Na^+ channels, present within CA1 apical dendrites, exhibit similar basic characteristics to those previously published for central neurons. The slope conductance reported here lies within the range of 10 to 17 pS reported for neuronal type Na^+ channels (Kirsch & Brown, 1989; Alzheimer *et al.* 1993). The voltage ranges of activation and inactivation are similar to those reported for CA1 neurons from whole-cell recordings (Sah *et al.* 1988; Steinhäuser, Tennigkeit, Matthies & Gündel, 1990). Also, the voltage dependence of activation and inactivation kinetics compares favourably with previous reports from CA1 neurons (Sah *et al.* 1988; Steinhäuser *et al.* 1990). No differences were observed in any of these properties between channels recorded from somatic and dendritic patches. A relatively constant number of Na^+ channels were found in patches recorded from the entire range of adult CA1 pyramidal apical dendrites. There may have been, however, a slight decrease in channel density for dendritic branches farther than 200 μm away from the soma. These data suggest that Na^+ channel density is fairly constant for most of the extent of CA1 dendrites. Dendritic Na^+ channels appear to be capable of alternating between transient, rapidly inactivating openings and later occurring, more prolonged openings. The presence of two distinct channel behaviours could underlie the two different rates of inactivation observed in ensemble averages. This channel behaviour has been hypothesized to be the result of a uniform population of channels switching between two different modes of gating. Bimodal gating has been described in detail for Na^+ channels recorded from several different cell types, including rat cortical neurons (Alzheimer *et al.* 1993; Taylor, 1993). As with cortical Na^+ channels, unitary current amplitude and slope conductance were the same for both types of channel opening recorded here. Based on this evidence it appears that a single type of Na^+ channel is responsible for both channel behaviours observed in CA1 apical dendrites. To date three distinct Na^+ channel subtypes have been described: types RI, RII, and RIII (Numann, Catterall & Scheuer, 1991; Taylor, 1993). It has been previously hypothesized that different channel subtypes are responsible for the different channel behaviours described above (Westenbroek *et al.* 1989). This seems unlikely in light of recent evidence which has shown that cloned type-I Na^+ channels exhibit very similar electrophysiology to that described for rat brain type-IIA Na^+ channels (Taylor, 1993).

Westenbroek *et al.* (1989) reported a differential distribution of Na^+ channel subtypes RI and RII in the CA1 region of the hippocampus. They showed that CA1 pyramidal somata were primarily labelled with antibodies specific for the RI Na^+ channel subtype while the highest immunoreactivity for RII subtype channels was found in stratum radiatum. From these data they suggested that CA1 somata contain mainly subtype RI and that the high RII labelling observed in stratum radiatum corresponds to a high density of RII subtype channels found in the axons of CA3 neurons. It is possible, however, that part of the RII labelling in stratum radiatum could be due to the labelling of CA1 dendrites. If this were the case, then a differential distribution of Na^+ channel subtypes, with somata containing mainly RI and axons and dendrites containing mainly RII, would exist in CA1 pyramidal neurons. The physiological significance of such a differential distribution is unknown.

Dendritic Ca^{2+} channels

The Ca^{2+} channels exhibiting a hyperpolarized range of activation and inactivation, prolonged single-channel openings of relatively small conductance, and very rapid ensemble current inactivation are reminiscent of T-type Ca^{2+} channels (Fox *et al.* 1987*b*; Fisher *et al.* 1990; O'Dell & Alger, 1991; Mogul & Fox, 1991). Most LVA Ca^{2+} channels, including those of hippocampal pyramidal neurons, present single-channel and whole-cell current characteristics that are very similar to those reported here. The pharmacological profile demonstrated by LVA channels varies somewhat depending upon cell type, but a sensitivity to amiloride and low concentrations of Ni^{2+} does appear to be the most consistent finding among the various types of LVA channels (Tang *et al.* 1988; Bean, 1989; Mogul & Fox,

1991). Such a pharmacological profile has been reported for LVA Ca^{2+} currents in rat hippocampal CA1 and CA3 pyramidal neurons, and the channels supporting these currents have been designated as T-type channels (Tang *et al.* 1988; Bean, 1989; Mogul & Fox, 1991). Thus, the above dendritic LVA Ca^{2+} channels exhibit both a biophysical and pharmacological profile very similar to those of the T-type Ca^{2+} channel.

There have been conflicting results with regard to the presence or absence of T-type channels in adult CA1 neurons. Several investigators have found no evidence of LVA channels in acutely isolated adult neurons (Kay & Wong, 1987; Thompson & Wong, 1991) while other groups have reported the presence of T-type channels in the pyramidal neurons of adult guinea-pig and rat (Fisher *et al.* 1990; Fisher & Johnston, 1990). Most studies do agree that T-channels are found on neurons isolated from neonatal animals (Thompson & Wong, 1991; O'Dell & Alger, 1991). The situation may be that, in CA1 pyramidal neurons of very young animals, T-type channels are distributed throughout the neuron and as the animal matures these channels become primarily localized to the dendritic arborizations. Although we have not made a detailed study of the relative distribution of somatic Ca^{2+} channels, the evidence presented here supports the idea that CA1 pyramidal dendrites contain a more dense population of T-type Ca^{2+} channels than the somatic regions of these neurons (see Fig. 11*C*).

HVA_m, moderately inactivating Ca^{2+} channels were also consistently found on the apical dendrites of CA1 pyramidal neurons. While this population exhibited a fairly homogenous set of biophysical characteristics, occasional channel activity that presented distinctly different unitary openings was encountered. An obvious difference was also observed in channel pharmacology. The main type of HVA_m channel appears to be a channel other than N-, P- or Q-type, as the presence of ω-conotoxin MVIIC did not affect the distinctive activity of these channels. The brief openings and reopenings exhibited by these channels were, however, blocked by 50 μM Ni^{2+} and by 1 mM amiloride. A similar pharmacological profile has been found for the R-type Ca^{2+} channels recorded in cerebellar neurons and for the possible counterparts of these native channels: the class E and doe-1 α_1 Ca^{2+} channel subunit clones (Soong *et al.* 1993; Ellinor *et al.* 1993*a*; Zhang *et al.* 1993; Schneider *et al.* 1994). This group of channels also exhibits unitary current amplitudes and conductances, voltage ranges of activation and inactivation, and inactivation time courses that are similar to those reported here for HVA channels in CA1 dendrites (Ellinor *et al.* 1993*a*; Zhang *et al.* 1993). Furthermore, Northern analysis has shown that abundant amounts of α_{1E} (rbE-II) mRNA are found in the adult rat hippocampus (Soong *et al.* 1993; Zhang *et al.* 1993). In light of this evidence, CA1 apical dendrites appear to contain a large complement of R-type Ca^{2+} channels, or at least a channel that exhibits similar characteristics when expressed in hippocampal neurons.

A subpopulation of HVA_m Ca^{2+} channel activity was also found in CA1 dendrites. While infrequent channel recordings precluded a definitive characterization, the unitary properties of these channels were very similar to those previously reported for N-type channels. As also has been shown for N-type channels, these dendritic channels were insensitive to low concentrations of Ni^{2+} and may have been ω-conotoxin sensitive. Based on these observations, it can be tentatively stated that a small population of N-type channels may be found in CA1 dendrites. It should be pointed out that Elmslie *et al.* (1994) have recently cast doubt on the idea that so-called N-type Ca^{2+} channels are the single-channel correlate of the ω-conotoxin-sensitive current in bullfrog ganglia. For the purposes of this paper, however, we will continue to refer to N-type channels as that channel activity which is inhibited by ω-conotoxins GVIA and MVIIC.

That we found only a subpopulation of N-type channels in CA1 dendrites was somewhat surprising given previous reports. A dense dendritic labelling by α_{1B} antibodies (CNB-1) or labelled ω-conotoxin has been reported in rat hippocampal slices and cultures (Westenbroek, Hell, Warner, Dubel, Snutch & Catterall, 1992; Mills *et al.* 1994). These studies suggest that N-type channels are quite abundant in the dendrites of hippocampal pyramidal neurons. This quantitative difference may arise as the result of some artifact introduced by cell-attached patch recordings from dendrites. The channels may be relatively inaccessible to the recording pipette or may not be active under our recording conditions. Alternatively, the immunolabelling of α_1-subunits may not be as specific for N-type channels as originally thought. In fact, a great deal of homology exists between the amino acid residues of class A, B and E α_1-subunits (Soong *et al.* 1993). Furthermore, these labelling studies do not preclude the presence of other large populations of Ca^{2+} channels in the dendrites of CA1 pyramidal neurons.

The HVA_1 Bay K 8644-sensitive Ca^{2+} channel has many characteristics of L-type channels described in detail for CA1 pyramidal neurons and for many other types of neurons (Nowycky *et al.* 1985; Fox *et al.* 1987*b*; Fisher *et al.* 1990; O'Dell & Alger, 1991). The relatively few recordings of this channel in dendritic patches distal to 50 μm from the soma, suggest that L-type channels are likely to be restricted to the soma and only the most proximal dendritic regions. These observations correspond well with previous studies that localized L-type channels to the soma and proximal dendrites (Westenbroek *et al.* 1990). There were, however, occasional L-type channels recorded from regions of the dendrites quite distal to the soma (up to 200 μm) demonstrating that a low density of L-type

channels may exist throughout the extent of CA1 apical dendrites.

The recordings presented here suggest that the apical dendrites of CA1 pyramidal neurons are primarily populated with T- and R-type channels, along with a lower level of N- and L-type channels. These findings are also consistent with recent fluorescence imaging experiments, undertaken in this laboratory, in which a similar distribution of channel types was observed (Christie, Eliot, Ito, Miyakawa & Johnston, 1995). The number of channels encountered in the present study was relatively constant throughout the extent of the dendritic arborization, and did not differ significantly from that found in a handful of somatic recordings. These results suggest that Ca^{2+} channel density is similar for all regions (excluding axonic and terminal regions) of CA1 pyramidal neurons. There were, however, substantial differences in the type of channels found within the somatic and dendritic regions of these neurons. The data from somatic patches reported here correspond well with previous reports from CA1 somata (Fisher *et al.* 1990; Thompson & Wong, 1991; Hillyard *et al.* 1992). We observed that T- and R-type channels are primarily localized in the apical dendrites while CA1 somata contain mainly L-, N- and Q-or P-type channels with fewer R- and T-type channels (see Fig. 11*C*). This differential distribution of Ca^{2+} channel types may have an important impact on the physiology of CA1 pyramidal neurons. The hyperpolarized activation voltage range of T-type channels endows these channels with the unique capability to be gated by relatively small depolarizations and provides them with a potentially important role in synaptic integration of CA1 neurons. On the other hand, the biophysical properties of R-type channels are shared by N-, and Q-type channels, and thus, it is not as clear what advantage these channels would have in shaping dendritic physiology over the other HVA, moderate conductance Ca^{2+} channel types.

Physiological significance of active dendrites

CA1 pyramidal neurons, as well as many other central neurons, receive many thousands of synaptic inputs that are widely distributed across the dendritic arborization. A large proportion of these synapses are both physically and electrotonically distant from the soma and also from other synapses (Andersen, Raastad & Storm, 1990). Cable filtering will act to reduce the amplitude of synaptic potentials and limit the amount of spatial summation that can occur between distributed synapses (Spruston *et al.* 1994). Active dendritic channels may thus provide a relatively straightforward mechanism by which the effect of electrotonically distant synaptic inputs can be amplified.

Dendritic Na^+ and Ca^{2+} channels are also well suited to play a critical role in shaping the firing behaviour of CA1 pyramidal neurons. Dendritic Na^+ channels have already been shown to enhance the backward propagation of somatically generated action potentials into the dendritic regions of cortical neurons (Stuart & Sakmann, 1994). This allows for more effective communication of the firing state of the output region of the cell (soma) with the input region (dendritic arborization). It is highly probable that such a process also occurs in CA1 pyramidal neurons although the extent of backpropagation may be more limited than in cortical neurons (Jaffe *et al.* 1992). Additionally, dendritic voltage-gated channels, particularly Ca^{2+} channels, have been hypothesized to play important roles in the generation of somatic bursting behaviour. Several modelling studies have shown the necessity of dendritic Ca^{2+} spikes for somatic burst generation (Traub, Miles & Jefferys, 1993). Such bursting activity has been proposed as a cellular mechanism for the genesis of prolonged epileptic events (Traub *et al.* 1993). Thus, dendritic active channels could play a role in both the basic physiological, as well as pathophysiological, electrical behaviour of neurons.

Finally, voltage-gated dendritic channels could elevate Ca^{2+} entry into dendrites, either directly through the opening of voltage-gated Ca^{2+} channels or indirectly by increasing relief of Mg^{2+}-blocked NMDA channels (Pongrácz *et al.* 1992; Jaffe *et al.* 1994). The central role of intracellular Ca^{2+} in regulating the various processes of synaptic plasticity is well documented. Ca^{2+} influx through voltage-gated channels has been shown to be capable of inducing a variety of short- and long-term modifications of synaptic strength in central neurons (Johnston *et al.* 1992; Linden, 1994). As long as the EPSP amplitude remains subthreshold, the influx of Ca^{2+} through active channels will be localized primarily to the area of synaptic input, providing a restricted space in which synaptic plasticity can take place (White, Levy & Steward, 1990; Jaffe *et al.* 1994). If action potentials are generated, however, this spatial domain of synaptic plasticity will be much more extensive. Thus voltage-gated channels in CA1 dendrites could be involved in the modification of synaptic strength by directly and indirectly affecting intracellular Ca^{2+} concentration.

In summary, these experiments provide direct evidence that CA1 dendrites contain a rich complement of inwardly conducting voltage-gated ion channels. The types of channels located within the dendrites are well suited to play integral roles in both synaptic integration and in the basic electrical behaviour of these neurons.

Alzheimer, C., Schwindt, P. C. & Crill, W. E. (1993). Modal gating of Na^+ channels as a mechanism of persistent Na^+ current in pyramidal neurons from rat and cat sensorimotor cortex. *Journal of Neuroscience* **13**, 660–673.

Andersen, P., Raastad, M. & Storm, J. F. (1990). Excitatory synaptic integration in hippocampal pyramids and dentate granule cells. *Cold Spring Harbor Symposia on Quantitative Biology* **55**, 81–86.

ANDERSEN, P., STORM, J. & WHEAL, H. V. (1987). Thresholds of action potentials evoked by synapses on the dendrites of pyramidal cells in the rat hippocampus *in vitro*. *Journal of Physiology* **383**, 509–526.

BEAN, B. P. (1989). Classes of calcium channels in vertebrate cells. *Annual Review of Physiology* **51**, 367–384.

CHRISTIE, B., ELIOT, L. S., ITO, K., MIYAKAWA, H. & JOHNSTON, D. (1995). Different Ca^{2+} channels in soma and dendrites of hippocampal pyramidal neurons mediate spike-induced Ca^{2+} influx. *Journal of Neurophysiology* **73**, 2553–2558.

COLLING, S. B. & WHEAL, H. V. (1994). Fast sodium action potentials are generated in the distal apical dendrites of rat hippocampal CA1 pyramidal cells. *Neuroscience Letters* **172**, 73–76.

DELCOUR, A. H. & TSIEN, R. W. (1993). Altered prevalence of gating modes in neurotransmitter inhibition of N-type calcium channels. *Science* **259**, 980–984.

ELIOT, L. S. & JOHNSTON, D. (1994). Multiple components of calcium current in acutely dissociated dentate gyrus granule neurons. *Journal of Neurophysiology* **72**, 762–777.

ELLINOR, P. T., ZHANG, J.-F., RANDALL, A. D., ZHOU, M., SCHWARZ, T. L., TSIEN, R. W. & HORNE, W. A. (1993*a*). Functional expression of a rapidly inactivating neuronal Ca^{2+} channel. *Nature* **32**, 455–458.

ELLINOR, P. T., ZHANG, J.-F., RANDALL, A. D., ZHOU, M., SCHWARZ, T. L., TSIEN, R. W. & HORNE, W. A. (1993*b*). Functional expression of a rapidly inactivating neuronal calcium channel. *Nature* **363**, 455–458.

ELMSLIE, K. S., KAMMERMEIER, P. J. & JONES, S. W. (1994). Reevaluation of Ca^{2+} channel types and their modulation in bullfrog sympathetic neurons. *Neuron* **13**, 217–228.

FISHER, R. E., GRAY, R. & JOHNSTON, D. (1990). Properties and distribution of single voltage-gated calcium channels in adult hippocampal neurons. *Journal of Neurophysiology* **64**, 91–104.

FISHER, R. E. & JOHNSTON, D. (1990). Differential modulation of single voltage-gated calcium channels by cholinergic and adrenergic agonists in adult hippocampal neurons. *Journal of Neurophysiology* **64**, 1291–1302.

FOX, A. P., NOWYCKY, M. C. & TSIEN, R. W. (1987*a*). Kinetic and pharmacological properties distinguishing three types of calcium currents in chick sensory neurones *Journal of Physiology* **394**, 149–172.

FOX, A. P., NOWYCKY, M. C. & TSIEN, R. W. (1987*b*). Single-channel recordings of three types of calcium channels in chick sensory neurones. *Journal of Physiology* **394**, 173–200.

HERRARAS, O. (1990). Propagating dendritic action potential mediates synaptic transmission in CA1 pyramidal cells In Situ. *Journal of Neurophysiology* **64**, 1429–1441.

HESS, P., LANSMAN, J. B. & TSIEN, R. W. (1986). Calcium channel selectivity for divalent and monovalent cations. Voltage and concentration dependence of single channel current in ventricular heart cells. *Journal of General Physiology* **88**, 293–319.

HILLE, B. (1984). In *Ionic Channels of Excitable Membranes*. Sinauer Associates Inc., Sunderland, MA, USA.

HILLYARD, D. R., MONJE, V. D., MINTZ, I. M., BEAN, B. P., NADASDI, L., RAMACHANDRAN, J., MILJANICH, G., AZIMI-ZOONOOZ, A., MCINTOSH, J. M., CRUZ, L. J., IMPERIAL, J. S. & OLIVERA, B. M. (1992). A new conus peptide ligand for mammalian presynaptic Ca^{2+} channels. *Neuron* **9**, 69–77.

JAFFE, D. B., JOHNSTON, D., LASSER-ROSS, N., LISMAN, J. E., MIYAKAWA, H. & ROSS, W. N. (1992). The spread of Na^{+} spikes determines the pattern of dendritic Ca^{2+} entry into hippocampal neurons. *Nature* **357**, 244–246.

JAFFE, D. B., ROSS, W. N., LISMAN, J. E., LASSER-ROSS, N., MIYAKAWA, H. & JOHNSTON, D. (1994). A model for dendritic Ca^{2+} accumulation in hippocampal pyramidal neurons based on fluorescence imaging measurements. *Journal of Neurophysiology* **71**, 1065–1077.

JOHNSTON, D., WILLIAMS, S., JAFFE, D. & GRAY, R. (1992). NMDA-receptor-independent long-term potentiation. *Annual Review of Physiology* **54**, 489–505.

KAY, A. R. & WONG, R. K. S. (1987). Calcium current activation kinetics in isolated pyramidal neurones of the CA1 region of the mature guinea-pig hippocampus *Journal of Physiology* **392**, 603–616.

KIRSCH, G. E. & BROWN, A. M. (1989). Kinetic properties of single sodium channels in rat heart and rat brain. *Journal of General Physiology* **93**, 85–99.

LINDEN, D. J. (1994). Long-term synaptic depression in the mammalian brain. *Neuron* **12**, 457–472.

LLINÁS, R., SUGIMORI, M., HILLMAN, D. E. & CHERKSEY, B. (1992). Distribution and functional significance of the P-type, voltage-dependent Ca^{2+} channels in the mammalian central nervous system. *Trends in Neurosciences* **15**, 351–355.

MCCLESKEY, E. W., FOX, A. P., FELDMAN, D. H., CRUZ, L. J., OLIVERA, B. M., TSIEN, R. W. & YOSHIKAMI, D. (1987). ω-Conotoxin: direct and persistent blockade of specific types of calcium channels in neurons but not muscle. *Proceedings of the National Academy of Sciences of the USA* **84**, 4327–4331.

MAGEE, J. C. & JOHNSTON, D. (1995). Synaptic activation of voltage-gated channels in the dendrites of hippocampal pyramidal neurons. *Science* **268**, 301–304.

MALENKA, R. C., KAUER, J. A., ZUCKER, R. S. & NICOLL, R. A. (1988). Postsynaptic calcium is sufficient for potentiation of hippocampal synaptic transmission. *Science* **242**, 81–84.

MAYER, M. L. & WESTBROOK, G. L. (1987). The physiology of excitatory amino acids in the vertebrate central nervous system. *Progress in Neurobiology* **28**, 197–276.

MILLS, L. R., NIESEN, C. E., SO, A. P., CARLEN, P. L., SPIGELMAN, I. & JONES, O. T. (1994). N-type Ca-channels are located on somata, dendrites, and a subpopulation of dendritic spines on live hippocampal pyramidal neurons. *Journal of Neuroscience* **14**, 6815–6824.

MINTZ, I. M., ADAMS, M. E. & BEAN, B. P. (1992). P-type calcium channels in rat central and peripheral neurons. *Neuron* **9**, 85–95.

MIYAKAWA, H. & KATO, H. (1986). Active properties of dendritic membrane examined by current source density analysis in hippocampal CA1 pyramidal neurons. *Brain Research* **399**, 303–309.

MIYAKAWA, H., ROSS, W. N., JAFFE, D., CALLAWAY, J. C., LASSER-ROSS, N., LISMAN, J. E. & JOHNSTON, D. (1992). Synaptically activated increases in Ca^{2+} concentration in hippocampal CA1 pyramidal cells are primarily due to voltage-gated Ca^{2+} channels. *Neuron* **9**, 1163–1173.

MOGUL, D. J. & FOX, A. P. (1991). Evidence for multiple types of Ca^{2+} channels in acutely isolated hippocampal CA3 neurones of the guinea-pig. *Journal of Physiology* **433**, 259–281.

NOWYCKY, M. C., FOX, A. P. & TSIEN, R. W. (1985). Long-opening mode of gating of neuronal calcium channels and its promotion by the dihydropyridine calcium agonist Bay K 8644. *Proceedings of the National Academy of Sciences of the USA* **82**, 2178–2182.

NUMANN, R., CATTERALL, W. A. & SCHEUER, T. (1991). Functional modulation of brain sodium channels by protein kinase C phosphorylation. *Science* **254**, 115–118.

O'Dell, T. J. & Alger, B. E. (1991). Single calcium channels in rat and guinea-pig hippocampal neurons. *Journal of Physiology* **436**, 739–767.

Ogata, N. & Tatebayashi, H. (1990). Sodium current kinetics in freshly isolated neostratial neurons of the adult guinea pig. *Pflügers Archiv* **416**, 594–603.

Pongrácz, F., Poolos, N. P., Kocsis, J. D. & Shepherd, G. M. (1992). A model of NMDA receptor-mediated activity in dendrites of hippocampal CA1 pyramidal neurons. *Journal of Neurophysiology* **68**, 2248–2259.

Rall, W., Burke, R. E., Holmes, W. R., Jack, J. J. B., Redman, S. J. & Segev, I. (1992). Matching dendritic neuron models to experimental data. *Physiological Reviews* **72**, S159–186.

Randall, A. D. & Tsien, R. W. (1995). Pharmacological dissection of multiple types of Ca^{2+} channel currents in rat cerebellar granule neurons. *Journal of Neuroscience* **15**, 2995–3012.

Regehr, W. G. & Tank, D. W. (1992). Calcium concentration dynamics produced by synaptic activation of CA1 hippocampal pyramidal cells. *Journal of Neuroscience* **12**, 4202–4223.

Richardson, T. L., Turner, R. W. & Miller, J. J. (1987). Action-potential discharge in hippocampal CA1 pyramidal neurons: current source-density analysis. *Journal of Neurophysiology* **58**, 981–996.

Sah, P., Gibb, A. J. & Gage, P. W. (1988). The sodium current underlying action potentials in guinea pig hippocampal CA1 neurons. *Journal of General Physiology* **91**, 373–398.

Sather, W. A., Tanabe, T., Zhang, J.-F., Mori, Y., Adams, M. E. & Tsien, R. W. (1993). Distinctive biophysical and pharmacological properties of class A (BI) calcium channel α_1 subunits. *Neuron* **11**, 291–303.

Schneider, T., Wei, X., Qin, N., Olcese, R., Neely, A., Constantin, J., Palade, P., Perez-Reyes, E., Smith, R. G., Appel, S. H., Stefani, E. & Birnbaumer, L. (1994). Molecular and functional characterization of human type E calcium channel. *Biophysical Journal* **66**, A423.

Sigworth, F. J. (1980). The variance of sodium current fluctuations at the node of ranvier. *Journal of Physiology* **307**, 97–129.

Soong, T. W., Stea, A., Hodson, C. D., Dubel, S. J., Vincent, S. R. & Snutch, T. P. (1993). Structure and functional expression of a member of the low voltage-activated calcium channel family. *Science* **260**, 1133–1136.

Spruston, N., Jaffe, D. & Johnston, D. (1994). Dendritic attenuation of synaptic potentials and currents: the role of passive membrane properties. *Trends in Neurosciences* **17**, 161–166.

Spruston, N., Schiller, Y., Stuart, G. & Sakmann, B. (1995). Activity-dependent action potential invasion and calcium influx into hippocampal CA1 dendrites. *Science* **268**, 297–300.

Steinhäuser, C., Tennigkeit, M., Matthies, H. & Gündel, J. (1990). Properties of the fast sodium channels in pyramidal neurones isolated from the CA1 and the CA3 areas of the hippocampus of postnatal rats. *Pflügers Archiv* **415**, 756–761.

Stuart, G. J., Dodt, H. U. & Sakmann, B. (1993). Patch-clamp recordings from the soma and dendrites of neurones in brain slices using infrared video microscopy. *Pflügers Archiv* **423**, 511–518.

Stuart, G. J. & Sakmann, B. (1994). Active propagation of somatic action potentials into neocortical pyramidal cell dendrites. *Nature* **367**, 69–72.

Swartz, K. J., Mintz, I. M., Boland, L. M. & Bean, B. P. (1993). Block of calcium channels in central and peripheral rat neurons by ω-conotoxin-MVIIC. *Society for Neuroscience Abstracts* **19**, 1478.

Tang, C.-M., Presser, F. & Morad, M. (1988). Amiloride selectively blocks the low threshold (T) calcium channel. *Science* **240**, 213–215.

Taylor, C. P. (1993). Na^+ currents that fail to inactivate. *Trends in Neurosciences* **16**, 455–460.

Thompson, S. M. & Wong, R. K. S. (1991). Development of calcium current subtypes in isolated rat hippocampal pyramidal cells. *Journal of Physiology* **439**, 671–689.

Traub, R. D., Miles, R. & Jefferys, J. G. R. (1993). Synaptic and intrinsic conductances shape picrotoxin-induced synchronized after-discharges in the guinea-pig hippocampal slice. *Journal of Physiology* **461**, 525–547.

Turner, R. W., Meyers, D. E. R. & Barker, J. L. (1989). Localization of tetrodotoxin-sensitive field potentials of CA1 pyramidal cells in the rat hippocampus. *Journal of Neurophysiology* **62**, 1375–1387.

Turner, R. W., Meyers, D. E. R. & Barker, J. L. (1993). Fast pre-potential generation in rat hippocampal CA1 pyramidal neurons. *Neuroscience* **53**, 949–959.

Turner, R. W., Meyers, D. E. R., Richardson, T. L. & Barker, J. L. (1991). The site for initiation of action potential discharge over the somatodendritic axis of rat hippocampal CA1 pyramidal neurons. *Journal of Neuroscience* **11**, 2270–2280.

Usowicz, M. M., Sugimori, M., Cherksey, B. & Llinás, R. (1992). P-type calcium channels in the somata and dendrites of adult cerebellar Purkinje cells. *Neuron* **9**, 1185–1199.

Westenbroek, R. E., Ahlijanian, M. K. & Catterall, W. A. (1990). Clustering of L-type Ca^{2+} channels at the base of major dendrites in hippocampal pyramidal neurons. *Nature* **347**, 281–284.

Westenbroek, R. E., Hell, J. W., Warner, C., Dubel, S. J., Snutch, T. P. & Catterall, W. A. (1992). Biochemical properties and subcellular distribution of an N-type calcium channel $\alpha 1$ subunit. *Neuron* **9**, 1099–1115.

Westenbroek, R. E., Merrick, D. K. & Catterall, W. A. (1989). Differential subcellular localization of the R_I and R_{II} Na^+ channel subtypes in central neurons. *Neuron* **3**, 695–704.

White, G., Levy, W. B. & Steward, O. (1990). Spatial overlap between populations of synapses determines the extent of their associative interaction during the induction of long-term potentiation and depression. *Journal of Neurophysiology* **64**, 1186–1198.

Winegar, B. D., Kelly, R. & Lansman, J. B. (1991). Block of current through single calcium channels by Fe, Co, and Ni. Location of the transition metal binding site in the pore. *Journal of General Physiology* **97**, 351–367.

Wong, R. K. S., Prince, D. A. & Basbaum, A. I. (1979). Intradendritic recordings from hippocampal neurons. *Proceedings of the National Academy of Sciences of the USA* **76**, 986–990.

Zhang, J.-F., Randall, A. D., Ellinor, P. T., Horne, W. A., Sather, W. A., Tanabe, T., Schwarz, T. L. & Tsien, R. W. (1993). Distinctive pharmacology and kinetics of cloned neuronal Ca^{2+} channels and their possible counterparts in mammalian CNS neurons. *Neuropharmacology* **32**, 1075–1088.

Acknowledgements

We thank Nelson Spruston, Greg Stuart, and Bert Sakmann for generously teaching us their techniques for patch clamping dendrites. We also thank Rick Gray and Robin Lester for comments on the manuscript. This work was supported by grants from NIH and National Institute of Mental Health (NIMH).

Received 16 September 1994; accepted 7 February 1995.